Prediction and analysis of excitation sources of car booming noise through a Bayesian meta-model

Gianluigi Brogna, Jérôme Antoni, Nicolas Totaro, Olivier Sauvage, Laurent Gagliardini

Journal Pre-proof

Prediction and analysis of excitation sources of car booming noise through a Bayesian meta-model

Gianluigi Brogna, Jérôme Antoni, Nicolas Totaro, Olivier Sauvage, Laurent Gagliardini

PII: S0022-460X(21)00300-X
DOI: https://doi.org/10.1016/j.jsv.2021.116228
Reference: YJSVI 116228

To appear in: *Journal of Sound and Vibration*

Received date: 31 October 2020
Revised date: 14 April 2021
Accepted date: 23 May 2021

Please cite this article as: Gianluigi Brogna, Jérôme Antoni, Nicolas Totaro, Olivier Sauvage, Laurent Gagliardini, Prediction and analysis of excitation sources of car booming noise through a Bayesian meta-model, *Journal of Sound and Vibration* (2021), doi: https://doi.org/10.1016/j.jsv.2021.116228

Prediction and analysis of excitation sources of car booming noise through a Bayesian meta-model

Gianluigi Brogna[a], Jérôme Antoni[a,*], Nicolas Totaro[a], Olivier Sauvage[b], Laurent Gagliardini[c]

[a] *Univ Lyon, INSA Lyon, LVA, EA677, 69621 Villeurbanne, France*
[b] *Stellantis N.V., Scientific and Future Technologies Department/StelLab, F-78140 Vélizy-Villacoublay, France*
[c] *Stellantis N.V., NVH Department, Route de Gisy, F-78140 Vélizy-Villacoublay, France*

Abstract

Current approaches in the automotive domain to predict booming noise essentially target extreme loading conditions. This is useful when mechanical strength is of concern, but not representative of the actual vehicle usage. Usage is however important when addressing acoustic annoyance. One issue in this respect is the lack of databases representative of the diversity of client usages and, therefore, of the excitation forces applied to the vehicle in real usage conditions. This paper introduces a possible answer to this problem. First, it proposes a measurement protocol to estimate the excitation forces in real usage responsible of booming noise. Second, it provides an array of algorithms to analyze the large amount of data collected during the measurement step. In particular, an *ad hoc* Independent Component Analysis algorithm is introduced to extract excitation components specific to well-defined operating condition regions, thus providing insights in the excitation behaviour, as well as data reduction. Next, the excitation components are modelled as a function of the vehicle operating conditions with a Radial Basis Function network. A meta-model of the excitations in real usage conditions is thus obtained, composed of two levels: the analysis level and the modelling level. The proposed methodology is developed in the Bayesian framework. In addition to its advantages linked to the trivial introduction of prior knowledge, the Bayesian framework is found particularly useful for propagating uncertainties throughout the successive steps of the approach.

Keywords: Booming noise; Load estimation; Independent component analysis; Radial basis functions network; Bayesian meta-model; Gibbs sampler

1. Introduction

The acoustic performance of a vehicle is a discriminating feature for the client. According to client's tastes, a car may have to sound sporty or smooth, or not to sound

*Jérôme Antoni
Email address: jerome.antoni@insa-lyon.fr (Jérôme Antoni)

at all. In order to consider such preference at minimum cost, the NVH (Noise, Vibration and Harshness) performance of vehicles is addressed as early as possible in the design process. Among the targeted NVH characteristics in internal combustion engine powered cars, the booming noise related to the engine dominates the low frequency band [1, 2] and is strictly linked to the client perception of quality [3]. A comprehensive approach to its prediction should take into account a large range of operating conditions (OCs) in order for it to be representative of the client perception. However, usual booming noise models seem to lack this completeness.

On the one hand, the classical approach is to synthesize the acoustic pressure linked to the booming noise by coupling the excitation sources with the vehicle frequency response functions (FRFs). While the estimation of these FRFs can be performed numerically, by finite element method (in the low frequency band) or statistical energy analysis (in the high frequency band) [4], the determination of the loads is more problematic. In theory, the inner load tensor of the engine can be obtained analytically and over the full operational range knowing the operating conditions and combustion parameters [5]. However, even when the excitation can be modelled analytically, it is so modelled in the active subsystem (the engine) and its application on the passive subsystem (for instance the car body) most of the times goes through some anti-vibration mounts. Unfortunately, these damping elements have often an unwell defined non-linear behaviour, so that the actual loads exciting the car body are basically unknown except at some very specific operating points for which the mount properties are known [6, 7]. This means that even if the FRFs can be estimated, a model of the loads injected in the car body is not available.

On the other hand, a purely "machine learning" take at booming noise prediction can be adopted by measuring the booming noise for several operating conditions and trying to build a model explaining the noise as a function of the OCs. Even if this approach shows promising results [8], the model so created is by no means general, but rather specific to the combination vehicle/power-train used to record the learning database.

In this context, this paper adopts a hybrid approach. A model of the excitation sources linked to the booming noise is built in a machine learning fashion from a large database of measured loads in operating conditions. Then, these loads are multiplied to the vehicle FRFs to yield a booming noise prediction. This has two main advantages:

- The definition of booming noise sources depend only on the power-train. This means that different car models sharing the same power-train will be affected by the same real usage excitations. This in turn reduces the number of measurements required to deal with several car models.
- Making the FRFs appear explicitly in the booming noise synthesis opens the path to more advanced FRFs estimation techniques that are able for instance to simulate the vehicle structural uncertainty due to the production dispersion (e.g. by non-parametric stochastic finite element approach [9]).

In order to alleviate the need of a large number of measurements to cover the whole operating condition range, the proposed approach consists in a meta-model composed of two stages: *analysis* with data reduction and *modelling*.

The analysis step is performed through an *ad hoc* Independent Component Analysis (ICA) algorithm. ICA is generally regarded as a way to extract from measurements independent phenomena. For instance, this makes it a valuable approach to identify hidden independent acoustic sources [10] or to perform Operational Modal Analysis [11, 12]. ICA is prone to extract sparse components, making it a particularly relevant for data reduction [13, 14]. In the context of this paper, ICA reveals all its value since, thanks to the sparsity of the components, it manages to identify loading *patterns* specific to well-defined operating conditions regions. However, its application to this aim is not straightforward. Therefore, a specific Bayesian version of ICA is proposed based on the formulations of Knuth and Djafari [15, 16].

Then, the second step aims at modelling the extracted independent components as a function of the vehicle OCs. The proposed approach is based on a Radial Basis Function (RBF) network. First developed in 1988 by Broomhead and Lowe [17], RBF networks are an interesting way of performing simple non-linear regression, which could approach as precisely as desired a target function. The Bayesian framework is again necessary in this step to take into consideration the uncertainty deriving from the data reduction in ICA.

Eventually, the complete model – hereafter referred to as the "meta-model" – will be used to simulate load scenarios corresponding to client usage. The full methodology is depicted in Fig. 1. It is resumed as follows: (1) a typical client usage of a vehicle described through vehicle OC distributions is taken as input, (2) the meta-model generates a population of independent components corresponding to the OCs input, (3) the meta-model recombines the components with extracted loading patterns to yield the loads, (4) finally, the synthesized loads are multiplied by the vehicle FRFs to yield an estimation of the booming noise representative of the client usage.

Moreover, the Bayesian approach adopted in this work allows the propagation of uncertainties through the successive steps listed in Fig. 1. As a consequence, the estimation of booming noise comes not only with point estimates, but also with credible intervals.

Note that the identified meta-model is specific to a power-train, which has to already be in the production phase since real usage measurements are necessary. However, in the automotive industry, a new car model rarely features a completely new power-train. This means that the meta-model can also be used in the early design stage of a new vehicle to predict its booming performance, given that the new vehicle features an existing power-train and that a computational model to estimate its FRFs exists. Otherwise, the proposed model can always be used for existing vehicles to compare two different client usage profiles with respect to their influence to the booming performance.

The paper is organized as follows. Section 2 covers a description of the vehicle system. First of all, the definition of the booming noise is clarified, along with the definition of the loads considered at its origin. Then, a brief sub-section covers the protocol to obtain the real usage excitation database, which is the input for the model building procedure. Section 3 targets the two levels of the meta-model, namely the ICA of the loads and the modelling of the extracted components. In this section, some basis of Bayesian modelling are also provided in order to introduce the framework in which the modelling is realised. Section 4 covers the exploitation of the identified meta-model. It first details the synthesis steps yielding a prediction of the booming noise. Then, it proposes an actual application and validates the model performance by comparing the

booming noise prediction to the actual measurement. A final conclusion is drawn on the advantages of the proposed approach, as well as on the difficulties one might encounter when applying it.

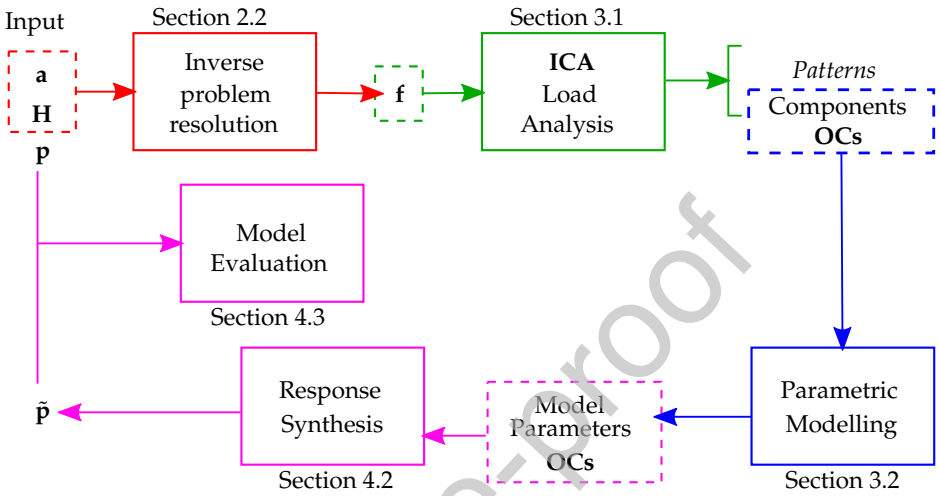

Figure 1: Explanatory diagram of the steps covered in the paper. In red the recovery of load **f** from measured accelerations **a** and given FRF matrix **H**, in green the load analysis, in blue the component modelling and in magenta the model synthesis and evaluation steps. The corpus of processing units that takes the operating conditions (OCs) as input and return the estimated pressure $\tilde{\mathbf{p}}$ in the cabin as output is referred to as the "meta-model".

2. Target system and input data

Let $\mathrm{p}(t,\omega)$ be the evolution along time t of the spectrum of the acoustic pressure inside a vehicle. On a low frequency range $[\omega_l, \omega_u]$, it can be considered composed of a wide-band part $\mathrm{p}_{wb}(t,\omega)$ and a harmonic part $\mathrm{p}^{(h_o)}(t)$ with respect to the engine speed ω_0:

$$\forall \omega \in [\omega_l, \omega_u], \quad \mathrm{p}(t,\omega) = \mathrm{p}_{wb}(t,\omega) + \sum_{o=1}^{O} \mathrm{p}^{(h_o)}(t)\delta(\omega - h_o\omega_0(t))/(h_o\dot{\omega}_0(t)), \quad (1)$$

where δ stands for the Dirac distribution and $\dot{\omega}_0(t) = d\omega_0(t)/dt$ is the engine acceleration.

The harmonic part of the acoustic pressure in Eq. (1) is commonly called booming noise and it is the key NVH issue in this paper. Largely covered in literature [3], the booming noise is pretty well defined. It is considered one of the most important contributions to the noise inside the cabin over a large low-frequency band and its structure-borne part is dominant with respect to the air-borne one. Several harmonics O can contribute to the noise inside the cabin and, typically for a 4-cylinder internal combustion engine, the most energetic ones are $h_o \in \{1, 2, 4, 6\}$.

The modelling of the excitation sources at the origin of the booming noise being the aim of this paper, a mechanical system covering the engine excitations to the vehicle body has to be defined.

2.1. The vehicle system

It is largely recognised that the loads at the origin of the booming noise come from the engine excitation [5]. However, the actual external loads generated in the engine can be hardly defined in terms of specific application points. As a consequence, the widely spread sub-structuring approach [18] is used in this paper. The vehicle system is considered composed of an active and a passive subsystems and the loads to estimate are the ones considered applied at the interface between the two subsystems. The decomposition is depicted in Fig. 2 and declined as follows:

- The active subsystem is composed of the engine (E) and the drive wheels[1] (A and B). The interface between the engine and the passive subsystem is located at the centres of the engine elastic mounts. Three loads are considered applied at each mount centre (1^{E_1}, 1^{E_2}, 1^{E_3}). The interface between the wheels and the passive subsystem is at the spindle bearings for the drive train. Three loads and two moments[2] are considered applied at each mount centre (1^{A}, 1^{B}).
- The rest of the car composes the passive sub-system (P).

As a consequence, $N_e = 19$ excitation degrees of freedom (DOFs) are here considered at the source of the booming noise inside the vehicle.

Once the active and passive subsystems and the excitation DOFs have been identified, the loads to estimate can be defined. If defined as the loads the active parts apply on the passive subsystem, then they correspond to the commonly called "operational" loads. If defined as external loads applied to the complete system at the above defined interfaces, then they rather correspond to the so-called "equivalent" loads [19]. Both definitions have their strong and weak points, however the "equivalent" loads are here preferred since:

- They only depend on the active sub-system, i.e. on the power-train. As explained in the introduction, this feature makes the model applicable to several different car models.
- They are associated with the frequency response functions of the whole system, therefore no dismounting is needed for the measurement of the FRFs (this is a characteristic problem of the "operational" loads).

Let $\mathbf{f}_1^{(h_o)}(t) \in \mathbb{C}^{N_e \times 1}$ be the vector containing the time evolution of the h_o-harmonic for the N_e excitations defined above. Then, in a linear mechanical system in which the equation of motion is verified, the h_o-harmonic pressure responses $\mathbf{p}_3^{(h_o)}(t) \in \mathbb{C}^{N_o \times 1}$ at observation DOFs 3 read:

$$\mathbf{p}_3^{(h_o)}(t) = \mathbf{H}_{31}(h_o\omega_0(t))\mathbf{f}_1^{(h_o)}(t)\,, \tag{2}$$

[1] The drive wheels are considered as sources as they are themselves excited by the engine harmonic torque ripple.

[2] The dynamic moment along the drive train direction is supposed null.

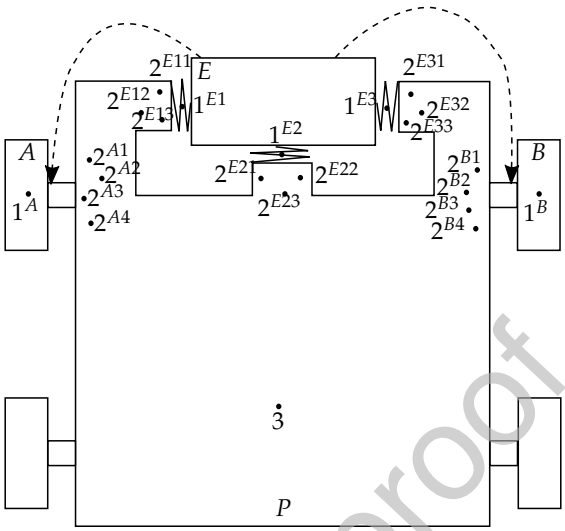

Figure 2: Decomposition of the vehicle system into an active subsystem (engine E, wheels A and B) comprising the main harmonic excitations and a passive subsystem P. Loads from the engine are transferred through mount centres 1^{E_1}, 1^{E_2}, and 1^{E_3}. Vibrations are measured at DOFs 2^{Ai}, 2^{Bi}, 2^{Eij} and pressure is measured at point 3 in the cabin. The dotted lines stand for the influence of the engine on the drive wheels through the drive-line.

where $\mathbf{H}_{31}(h_o\omega_0(t)) \in \mathbb{C}^{N_o \times N_e}$ stands for the FRF matrix between the N_e excitations and the N_o responses. Note that the FRFs are linear time invariant (as functions of $h_o\omega_0$) and their dependence with time is due to the fact that an harmonic instantaneous frequency changes in time with the engine speed $\omega_0(t)$.

The aim now is to identify the excitation $\mathbf{f}_1^{(h_o)}(t)$ in real usage, i.e. while the vehicle operating conditions change in time. This in turn will allow a model of the excitations as a function of the OCs to be built from the collected database.

2.2. *Real driving load estimation*

Unfortunately, the direct measurement of the loads $\mathbf{f}_1^{(h_o)}(t)$ in real usage conditions is impossible. It can be shown that it can only be achieved clamping the active part to a rigid test bench [19]. While this kind of measurement is currently performed in the automotive domain [20, 21], it necessarily needs the active part to be dismantled from the system, thus compromising the "real usage" constraint needed in this work. As a consequence, the indirect in-situ approach is preferred here [22, 23].

Let $\mathbf{a}_2^{(h_o)}(t) \in \mathbb{C}^{N_a \times 1}$ be the vector containing the time evolution of the h_o-harmonic for N_a acceleration DOFs. In the vehicle system, they can be written as a function of the excitations as:

$$\mathbf{a}_2^{(h_o)}(t) = \mathbf{H}_{21}(h_o\omega_0(t))\mathbf{f}_1^{(h_o)}(t)\,, \tag{3}$$

where $\mathbf{H}_{21}(h_o\omega_0(t)) \in \mathbb{C}^{N_a \times N_e}$ stands for the FRF matrix between the N_e excitations and the N_a learning DOFs. If the FRFs in $\mathbf{H}_{21}(h_o\omega_0(t))$ are known (computed or measured)

and if during the real usage test the accelerations $\mathbf{a}_2^{(h_o)}(t)$ are measured, then Eq. (3) can be inverted at each instant t and the excitations $\mathbf{f}_1^{(h_o)}(t)$ recovered. This in-situ approach allows the identification of the loads in the whole mechanical system without any need for dismounting it. Thus, it is especially indicated for real usage tests.

2.2.1. Inverse problem

Solving the aforementioned inverse problem is far from trivial. First of all, the inversion of the transfer matrix requires $\mathbf{H}_{21}(h_o\omega_0(t))$ to be full rank (at each time instant). In order to ensure this constraint, the number of learning DOFs is taken larger than the number of excitations to be estimated ($N_a > N_e$). Therefore, 4 triaxial accelerometers have been placed around each spindle and 3 triaxial accelerometers around each engine mount, for a total of $N_a = 51$ learning DOFs to estimate 19 excitation.

The overdetermined problem can then be solved using the Moore-Penrose pseudo-inverse, which returns the minimum norm solution,

$$\forall t, \quad \mathbf{f}_1^{(h_o)}(t) = \left(\mathbf{H}_{21}(h_o\omega_0(t))^H\mathbf{H}_{21}(h_o\omega_0(t))\right)^{-1}\mathbf{H}_{21}(h_o\omega_0(t))^H\mathbf{a}_2^{(h_o)}(t)\,, \tag{4}$$

where $\bullet^H$ stands for the Hermitian transpose.

However, even with an overdetermined problem, one has to pay attention to the conditioning of matrix $\mathbf{H}_{21}(h_o\omega_0(t))$. An ill conditioned FRF matrix would make the estimation utterly sensitive to measurement noise. For this reason, *regularization* techniques are normally used. They consist in modifying slightly the original problem in order to obtain a more stable one.

A review of all regularization methods is not in the scope of this paper, but simply note that several approaches exist and among them the most used are the Tikhonov regularization and the Truncated Singular Value Decomposition [24]. They perform usually well and are easy to use, but the degree of regularization these methods impose is purely mathematical and endless discussion exists to find out the best method to choose the value of the regularization parameter (today one of the most used approaches is the *L-curve* [25]).

In this paper, the loads to be modelled have been obtained through a completely different method. The inverse problem has been formulated in the Bayesian framework and a probabilistic estimation of the loads has been carried out. Such an approach has a double advantage over the classic ones. First of all, the Bayesian context allows prior knowledge and information to be used as a way of regularizing the problem through "physical" considerations. Secondly, the probabilistic take at load estimation yields not only a deterministic result, but full probability distributions, thus yielding also credible intervals on the results. Already proposed by Calvetti [26], this method has been further developed in the context of force reconstruction by Aucejo and Feng [27, 28]. The results of its application on the database used for the present paper can be found in [29].

Knowing the way to estimate the loads $\mathbf{f}_1^{(h_o)}(t)$, what is left is to define the measurement protocol which shall yield the load database necessary to perform the modelling.

2.2.2. Measurement protocol

Looking at Eqs. (3) and (4) it seems clear that the load estimation needs the measurement of the FRF matrix $\mathbf{H}_{21}(h_o\omega_0(t))$ and of the real usage accelerations $\mathbf{a}_2^{(h_o)}(t)$. The

measurements cover only the low frequency range [20, 250] Hz. This range is enough to fully analyse the booming noise contribution of the main orders $h_o \in \{1, 2, 4, 6\}$ in a 4-cylinders Diesel engine.

FRF measurements. The FRF matrix were measured once at still vehicle and for the whole frequency range, since it is considered invariant with the operating conditions[3]. Two types of FRFs were measured: vibro-acoustical, from the excitation DOFs noted 1^{Ei} in Fig. 2 toward the microphones inside the vehicle cabin at point 3 (used for synthesis in Eq. (2)), and vibratory, from the same excitation DOFs toward the observation DOFs noted 2^{Ai}, 2^{Bi} and 2^{Eij} in Fig. 2 (used for load estimation in Eq. (3)). The former were measured by reciprocity [30], using sound sources at 3 and measuring the acceleration response at 1. The latter were measured by direct method, applying a hammer impact on 1 and measuring the accelerations at 2. Each measurement has been realized three times and the empirical mean is taken as a result. The hypothesis of local rigid body motion needed for this approach has been verified for the studied interfaces and it holds well above 250 Hz.

Acceleration measurements. This second protocol provides the acceleration measurements needed to solve the inverse problem (2). It has to cover different vehicle life situations, in order to build a complete database of the loads injected in a car during its usage. As a consequence, it needs to be applicable in a moving vehicle. The acquisition system records all the accelerations at the learning DOFs 2, which have been fitted with accelerometers (adapted to withstand real driving conditions). At the same time, the vehicle cabin was equipped with 4 microphones. For what concerns the vehicle operating conditions, they have been recorded directly from the **CAN** (Controller Area Network) bus of the vehicle (Fig. 3). The complete list of recorded channels can be seen in table 1.

In order to cover the widest operating conditions range possible with a reasonable agenda, different tests have been realized. For instance, acceleration/coast tests are useful to cover all the torque and engine speed ranges, while circuit tests aim at driving the car like a "normal" customer would and give an image of the range of all the operating conditions during a common vehicle usage.

All results in the following sections have been obtained from data of the circuit test and concern the second harmonic h_2, the most energetic ones when dealing with four cylinders engines.

[3] Note that the time invariant hypothesis is not completely verified, since the FRFs are slightly influenced by the dynamical behaviour of the vehicle. However, FRFs in driving conditions are much more complex to obtain and are not in the scope of this work.

Triaxial Accelerometers		Microphones	
Place	n. of accelerometers	Place	n.
Right mount 2^{E_3}	3	Cabin	4
Bottom mount 2^{E_2}	3		
Left mount 2^{E_1}	3		
Right mount (on engine)	1		
Bottom mount (on engine)	1		
Left mount (on engine)	1		
Front left wheel 2^{A}	4		
Front right wheel 2^{B}	4		

GPS	**CAN** data
Speed	Vehicle speed
North Velocity	Engine speed
East Velocity	Torque
Up Velocity	Wheel angle
Latitude	Gear
Longitude	Throttle
Altitude	Temperatures

Table 1: List of the data recorded for the harmonic noise protocol.

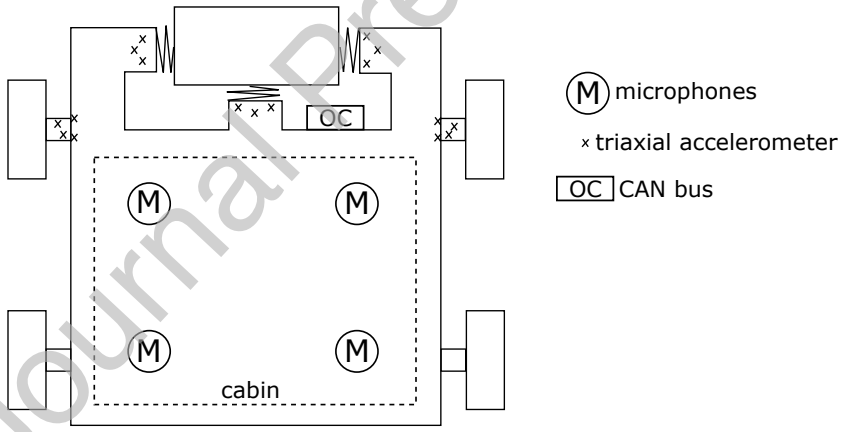

Figure 3: For the harmonic protocol 3 triaxial accelerometers have been placed at each engine mount (body side) and 4 at each front wheel hub. Inside the cabin, the acoustic pressure is measured thanks to 4 microphones. The operating conditions of the vehicle are recorded directly from the **CAN** bus.

3. Meta-model

The measurement protocols and processing steps intriduced in Section 2 yield a real driving condition database of the loads responsible for the booming noise. For each load sample, the corresponding OCs have been measured as well. However, modelling

and interpreting each of the $N_e = 19$ excitations can be cumbersome. Therefore, the proposed model features two stages (Fig. 4):

- In the first stage a probabilistic factor analysis deals with data reduction and analysis. The N_e loads are therefore described through a few independent components, which have the property to be dominant on well-defined OC regions.
- The second stage tackles the modelling of the components obtained at the previous step as a function of the vehicle operating conditions.

The probabilistic Bayesian approach is deemed here valuable to estimate the uncertainties introduced in the factor analysis stage and to propagate them to the modelling step.

In what follows each stage is detailed.

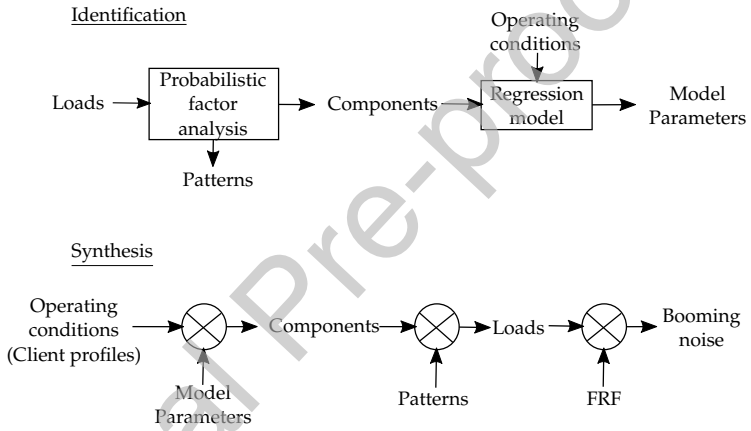

Figure 4: Depiction of the proposed meta-model in its identification and then exploitation to estimate the booming noise.

3.1. *Probabilistic factor analysis*

3.1.1. *Definition of the problem*

The first aim of the factor analysis stage is to describe the loads through a small number of components, thus easing the interpretation.

Let N_c ($N_c \leqslant N_e$) be the number of component extracted; a reduced version of the loads is sought in the following form:

$$\mathbf{f}_1^{(h_o)}(t) = \sum_{i=1}^{N_c} \boldsymbol{\lambda}_i \gamma_i(t) + \mathbf{r}(t)\,, \tag{5}$$

where the loads are expanded as a sum of contributions due to the components $\gamma_i(t) \in \mathbb{C}$ multiplied by what will be hereafter called excitation *patterns* $\boldsymbol{\lambda}_i \in \mathbb{C}^{N_e \times 1}$. The *patterns* contain the magnitude and phase relations among the excitation DOFs and are not time dependent; the time evolution is rather described through the corresponding

components $\gamma_i(t)$. Moreover, the number N_c of extracted components is usually less than the number N_e of excitations, thus performing data reduction, but also yielding a reconstruction error $\mathbf{r}(t)$.

The second aim of the factor analysis is linked to the nature of the components. Indeed, it must be noted that the decomposition in Eq. (5) is not unique: an infinity of bases are available to extract the components. As a consequence, several techniques exist in the literature in order to impose some kind of constraint and yield a unique pertinent decomposition[4]. In the context of this study, the components are wished to be dominant over well-defined operating condition regions. This would yield significant knowledge to solve engineering problems, since, in a given operating condition region, only one *pattern* describes the excitation.

The way to answer this need is not straightforward. It is recognised that the decomposition performed under the constraint of statistical independence among the components leads to sparse components, i.e. components dominating only on small regions of the sampled dimension [13]. However, this means that using Independent Component Analysis (ICA) [31] directly on $\mathbf{f}_1^{(h_o)}(t)$ would yield components dominating on small time regions, not OC regions. To solve this problem, it is proposed here to re-sample the loads along the operating conditions and then apply ICA to the re-sampled data. The loss of the time domain structure is not detrimental for the definition of the meta-model which is the aim of this paper, however it will be shown that the re-sampling step is not properly defined and entails the introduction of an error. The Bayesian formulation of the ICA is then necessary to take into account this error.

Hereafter, the algorithms used to achieve both aims are presented. First of all, data reduction is performed by Singular Value decomposition. A change of variable is then necessary to consider the so-reduced loads as samples in the operating condition domain, rather then in the time domain. Finally, Bayesian ICA manages to yield components dominant only on well-defined OC regions.

3.1.2. Step 1: Data reduction

Let $\mathbf{F} \in \mathbb{C}^{N_e \times N}$ be the matrix containing the N time samples of $\mathbf{f}_1^{(h_o)}(t)$, where it is assumed that $N \geqslant N_e$.

First of all, the matrix $\mathbf{F}$ can be expressed as:

$$\mathbf{F} = \mathbf{\Lambda}^{\bullet}\mathbf{C}^{\bullet} = \sum_{i=1}^{N_e} \boldsymbol{\lambda}_i \boldsymbol{\gamma}_i \,, \tag{6}$$

where $\mathbf{\Lambda}^{\bullet} \in \mathbb{C}^{N_e \times N_e}$ and $\mathbf{C}^{\bullet} \in \mathbb{C}^{N_e \times N}$ are the matrices storing *patterns* and components without any reduction (the number of components N_c is equal here to N_e). This relation can be rewritten as a sum of the contributions of each component, given that $\boldsymbol{\lambda}_i$ is the i^{th} column of matrix $\mathbf{\Lambda}^{\bullet}$ and $\boldsymbol{\gamma}_i$ is the i^{th} row of matrix $\mathbf{C}^{\bullet}$.

As for Eq. (5), the decomposition in Eq. (6) is not unique. As a consequence, a decorrelation constraint among the components can for instance be added. This constraint yields the *principal* components [32] and reads:

$$\mathbf{C}^{\bullet}\mathbf{C}^{\bullet\,H} = \mathbb{I}_{N_c} \,. \tag{7}$$

[4]For instance, one of the most widespread is the Principal Component Analysis, which imposes the decorrelation among the components.

Now the deterministic resolution is straightforward. One computes:

$$\mathbf{S} = \mathbf{F}\mathbf{F}^H = \mathbf{V}\mathbf{D}^{1/2}\mathbf{D}^{1/2}\mathbf{V}^H\,, \tag{8}$$

where $\mathbf{V} \in \mathbb{C}^{N_e \times N_e}$ and $\mathbf{D} \in \mathbb{C}^{N_e \times N_e}$ are respectively the matrix of the eigenvectors and the diagonal matrix of the eigenvalues of $\mathbf{S}$. Also, from Eq. (7):

$$\mathbf{S} = \mathbf{F}\mathbf{F}^H = \mathbf{\Lambda}^\bullet \mathbf{C}^\bullet \mathbf{C}^{\bullet\,H} \mathbf{\Lambda}^{\bullet\,H} = \mathbf{\Lambda}^\bullet \mathbf{\Lambda}^{\bullet\,H}\,. \tag{9}$$

By identification of Eqs. (8) and (9), $\mathbf{\Lambda}^\bullet$ is determined and so $\boldsymbol{\lambda}_i$ and $\boldsymbol{\gamma}_i$ for all $i \in \{1, \ldots, N_e\}$.

Data reduction is achieved keeping a reduced number of components $\boldsymbol{\gamma}_i$ to perform the recomposition in Eq. (6). Classically in Principal Component Analysis, the eigenvalues in matrix $\mathbf{D}$ are ordered by decreasing value and the "first" N_c components are kept - i.e. the components related to the N_c "most energetic" eigenvalues, with N_c chosen through a threshold on the cumulative sum of eigenvalues. This is a good protocol to minimize the number of components necessary to describe the loads with a certain degree of precision. In this work however, one final quantity to predict is the vehicle response. So, assuming that the global acoustic response is the priority, another cost function can be defined.

Let $\mathbb{S}$ be the set of all the components, so that $\mathbb{S}$ has N_e elements. Let $\mathbb{P}_S$ be the set of all possible combinations $\binom{N_e}{k}$ for all $k \in \{1, \ldots, N_e\}$. Noting $N_c^{(set)}$ one of the possible combinations, the minimization problem becomes:

$$N_c^{(opt)} = \underset{N_c^{(set)} \in \mathbb{P}_S}{\operatorname{argmin}} \left| \frac{1}{N_o N} \sum_{m=1}^{N_o} \sum_{n=1}^{N} |\overline{L}_{m,n} - L_{m,n}^{N_c^{(set)}}|^2 - L_{thr} \right|\,, \tag{10}$$

where $\overline{L}_{m,n}$ is the acoustic level at one of the N_o observation DOFs 3 recomposed from the identified loads with Eq. (2), while $L_{m,n}^{N_c^{(set)}}$ is the same level but computed using the loads after reduction through the $N_c^{(set)}$ components. The threshold for the data reduction is chosen by the user through L_{thr}. The higher the threshold, the higher the data reduction and consequently the reconstruction error. In practice, the set $\mathbb{P}_S$ is extremely wide and not all possible combinations can be tested. In order to find a good combination, an iterative algorithm starts with the full set of components $\mathbb{S}$ and one by one removes those that have the least contribution to the acoustic pressure. Applied to the circuit test load database, this approach returns the approximation $\tilde{\mathbf{F}}$ of the matrix $\mathbf{F}$ as:

$$\tilde{\mathbf{F}} = \sum_{i \in N_c^{(algo)}} \boldsymbol{\lambda}_i \boldsymbol{\gamma}_i\,, \tag{11}$$

with $N_c^{(algo)}$ of size $N_c = 7$ for $L_{thr} = 3$ (Fig. 5).

It is important to note that this data reduction has indeed a physical meaning. As explained in Section 2, the loads responsible for the booming noise are strictly linked to the engine excitation. A running engine state is mainly described through only two parameters: its speed and torque. Reality is certainly more complex, but a high degree of data reduction at this stage seems completely within expectations.

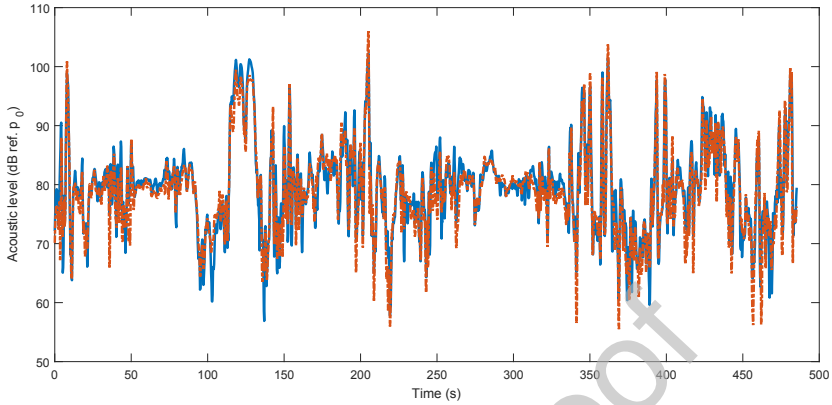

Figure 5: Comparison between the second harmonic h_2 of the acoustic pressure at the driver's ears recomposed using the loads estimated by inverse method (blue solid line) and using the loads after reduction with $N_c = 7$ (red dashed line). The curves are smoothed over 1 s.

3.1.3. *Step 2: Change of variables*

The matrix $\tilde{\mathbf{F}}$ now contains a reduced version of the load time samples. The aim of the change of variable is to rewrite the loads in the operating condition domain, instead of the time domain.

Let $\mathbb{T}$ be the smooth manifold for the time and $\mathbb{O}$ the one for the operating conditions. A *regular variable substitution* is the map $\mathbf{\Pi}$ so that $\mathbf{\Pi} : \mathbb{T} \rightarrow \mathbb{O}$ is continuous and bijective. If this map exists, a direct change of variable can be performed.

In the harmonic case, one might restrain the operating condition domain to the engine torque and speed only[5]. In this case, the domain becomes $\mathbb{O} : [T_{min}, T_{max}] \times [R_{min}, R_{max}]$ with T_{min} and R_{min} standing for the minimum engine torque and speed during the test and T_{max} and R_{max} the maximum of the same quantities.

In practice, in the discretized context, the manifold $\mathbb{O}$ is gridded and separated in torque/speed bins. Then, knowing the values of the engine torque and speed at each measured temporal sample (during the drive test), the map $\mathbf{\Pi}$ is empirically built. Unfortunately this map does not comply with the theoretical conditions above, due to two main problems both shown in Fig. 6:

- The map is not bijective since some torque/speed bins are "visited" more than once during the drive test (Fig. 6(a));
- The manifold $\mathbb{O}$ is not smooth (or dense) since the loads are not defined on all the torque/speed bins, i.e. some bins have not been "visited" during the test (Fig. 6(b)).

[5]The harmonic source is the engine and the engine operating conditions are globally described by its torque delivery and speed.

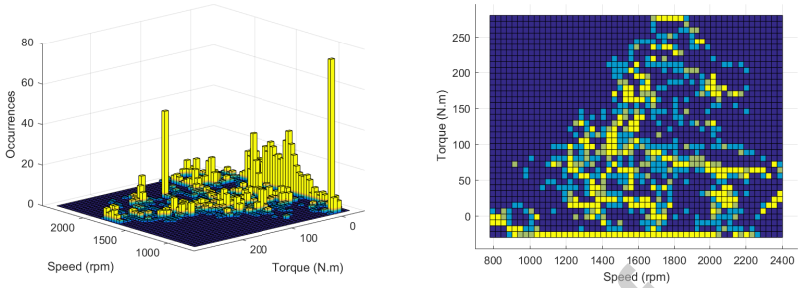

(a) (b)

Figure 6: Histogram of the engine torques and speeds covered during the driving test. (a) shows the occurrences, (b) the torque/speed pairs covered.

To solve the second problem one just has to map $\mathbb{T}$ towards another manifold $\mathbb{O}'$ composed of only the "visited" torque/speed bins, thus yielding to a reduced bin number $N_{bins} = 801$. This solution is simple, but it has to be reminded that operations such as interpolation or extrapolation loose all their physical meaning since two neighbour points in this domain may correspond to two completely different torque/speed pairs.

For the first problem an original solution is proposed. Instead of forcing the one-to-one correspondence between the two domains, all occurrences in the torque/speed bins are kept. As a consequence, a new structure for the reduced loads $\tilde{\mathbf{F}}$ is defined as $\{\tilde{\mathbf{F}}\} = \{\tilde{\mathbf{F}}^{(1)}, \ldots, \tilde{\mathbf{F}}^{(N_{bins})}\}$, with N_{bins} the number of "visited" torque/speed bins. For each $s \in \{1, \ldots, N_{bins}\}$, $\tilde{\mathbf{F}}^{(s)} \in \mathbb{C}^{N_e \times N_s^{(s)}}$ is the matrix containing the $N_s^{(s)}$ occurrences in the torque/speed bin s of the complex harmonic amplitude of the N_e reduced loads. Keeping all occurrences in each bin, the fundamental information stored in this structure is the dispersion inside each bin (Fig. 7). This dispersion is meant to be directly taken into account in the Bayesian ICA presented in the next paragraph.

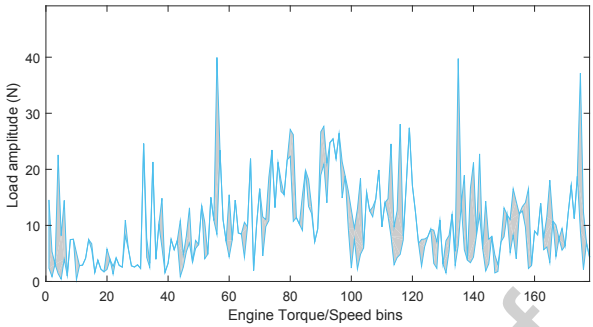

Figure 7: Evolution of the second harmonic h_2 of the load at the right engine mount Z direction along the torque/speed bins (zoom on the first 180 bins). The grey area depicts the bins where more occurrences are available and stands for the gap between the highest and lowest amplitude value.

3.1.4. Step 3: Bayesian ICA

The problem to be solved in the Bayesian ICA step is equivalent to the one in Eq. (5), but now carried out on the resampled loads in the structure $\{\tilde{\mathbf{F}}\}$. Let $\hat{\mathbf{F}} \in \mathbb{C}^{N_e \times N_{bins}}$ be the matrix containing the mean of the load occurrences for each engine torque/speed bins. It thus reads:

$$\forall s = 1, \dots, N_{bins}, \quad \hat{\mathbf{F}}_{:,s} = \frac{1}{N_s^{(s)}} \sum_{p=1}^{N_s^{(s)}} \tilde{\mathbf{F}}_{:,p}^{(s)} \,. \tag{12}$$

The aim is to decompose $\hat{\mathbf{F}}$ as:

$$\hat{\mathbf{F}} = \hat{\mathbf{\Lambda}}\hat{\mathbf{C}} + \hat{\mathbf{R}} = \sum_{i=1}^{N_c} \hat{\boldsymbol{\lambda}}_i \hat{\boldsymbol{\gamma}}_i + \hat{\mathbf{R}} \,, \tag{13}$$

where $\hat{\boldsymbol{\lambda}}_i \in \mathbb{C}^{N_e \times 1}$ are the *patterns*, $\hat{\boldsymbol{\gamma}}_i \in \mathbb{C}^{1 \times N_{bins}}$ are the corresponding components and $\hat{\mathbf{R}} \in \mathbb{C}^{N_e \times N_{bins}}$ is a reconstruction error. The matrices $\hat{\mathbf{\Lambda}}$ and $\hat{\mathbf{C}}$ store respectively the *patterns* and the components and, together with the error $\hat{\mathbf{R}}$, are the target of estimation.

First of all, note that the number of components extracted is fixed to the previously defined N_c. This means that this step does not search additional reduction, but rather an analysis of the already reduced loads.

Secondly, as usual this decomposition is not unique. A well-chosen constraint is sought in order to unequivocally define the components and *patterns* so that the former are sparse and dominant only on small engine torque/speed regions. Such a constraint appears to be the statistical independence of the extracted components. Largely covered in literature [31, 13], it is a stronger conditions than decorrelation and it needs the loads $\hat{\mathbf{F}}$ to be considered as a collection of N_{bins} samples of a stochastic load vector. In this context, the components $\hat{\boldsymbol{\gamma}}_i$ are themselves a collection of samples of stochastic variables $\hat{\gamma}_i$. Their independence can then be properly defined resorting to the separability of the joint probability density function (PDF) of the components. The components $\hat{\gamma}_i$ are

independent if and only if:

$$[\hat{\gamma}_1, \ldots, \hat{\gamma}_{N_c}] = \prod_{i=1}^{N_c} [\hat{\gamma}_i] \,, \tag{14}$$

where $[\hat{\gamma}_i]$ stands for the PDF of the component $\hat{\gamma}_i$ and $[\hat{\gamma}_1, \ldots, \hat{\gamma}_{N_c}]$ for the joint PDF of all components. In practice, such constraint can be enforced in several different ways. A wide review of these approaches can be found in Hyvarinen's book [31]. In the context of our work, it must be reminded that the input data $\hat{\mathbf{F}}$ actually comes already with a dispersion, described by the structure $\{\tilde{\mathbf{F}}\}$. For this reason, the estimation of the independent components and respective *patterns* is here carried out in the Bayesian context.

In the Bayesian framework, every term in Eq. (13) has to be considered as a random variable and the problem is thus rewritten as:

$$\hat{\mathcal{F}} = \hat{\Lambda}\hat{\mathcal{C}} + \hat{\mathcal{R}} \,, \tag{15}$$

where $\hat{\mathcal{F}}$ is a random term whose available data is $\hat{\mathbf{F}}$, whereas $\hat{\Lambda}$, $\hat{\mathcal{C}}$ and $\hat{\mathcal{R}}$ are the random terms respectively describing the *patterns*, the components and the error. The aim is to estimate the posterior PDF of $\hat{\Lambda}$ and $\hat{\mathcal{C}}$ knowing the data $\hat{\mathbf{F}}$. To do so by Bayes theorem, the likelihood function and prior distributions are needed.

The likelihood of $\hat{\mathbf{F}}$ is linked to the error hypothesis. It is reminded that the likelihood corresponds to the PDF of the data, for given values of the unknown random variables. In this application, if $\hat{\Lambda}$ and $\hat{\mathcal{C}}$ are considered as fixed, Eq. (15) shows that the only random influence to the data comes from the error $\hat{\mathcal{R}}$. Classically, $\hat{\mathcal{R}}$ is supposed to follow a circularly symmetric complex Gaussian distribution, being it a plain data reduction error. Under this assumption and given a value for the components and *patterns*, the likelihood reads:

$$[\hat{\mathbf{f}}_v | \hat{\Lambda}, \hat{\mathcal{C}}, \sigma^2_{f_{1,1}}, \ldots, \sigma^2_{f_{N_e,N_{bins}}}] \sim \mathcal{N}\left(\hat{\boldsymbol{f}}_v, \begin{bmatrix} \sigma^2_{f_{1,1}} & & \\ & \ddots & \\ & & \sigma^2_{f_{N_e,N_{bins}}} \end{bmatrix} \right) \,, \tag{16}$$

where $\hat{\mathbf{f}}_v$ is the vectorization of $\hat{\mathbf{F}}$, whereas $\hat{\boldsymbol{f}}_v$ is the vectorization of the product $\hat{\Lambda}\hat{\mathcal{C}}$. Note that the error has been supposed Gaussian, but this does not mean that its unknown variance is supposed the same for each excitation DOF and sample. Instead, it is allowed to be different in order to account for important error on specific DOFs and torque/speed bins. In particular, admitting different variances along the sample dimension is commonly referred to as Scaled Mixture Of Gaussians (SMOG) modelling [33] and it is here necessary to properly propagate the dispersion described by the structure $\{\tilde{\mathbf{F}}\}$. This being said, note that this increased precision in the model comes at a price: instead of inferring one global variance for the noise, $N_e \cdot N_{bins}$ variances have to be inferred, thus implying an increased computational cost.

Now that the likelihood function has been defined, another ingredient is necessary for the application of Bayes rule: the prior PDFs. They are chosen by the analyst and mirror the knowledge he/she has on the random variables to infer prior to taking into account of the measurements or input data. One first way to convey information is the family of distribution. For instance, if no information is available, usually uniform

distributions are used. On the other hand, if we know that the random variable has positive support (as variances for instance), then positive distributions can be used, such as Gamma or Inverse Gamma. Once the family of distribution is chosen, some more information can be conveyed by choosing the distribution parameters accordingly. For instance, the analyst could have an idea of the mean value of the inferred variable even before the measurements are accounted for. In this case, this knowledge is conveyed by fixing the mean of the prior PDF to the analyst's believed value. On the other hand, if no information on the prior PDF parameters is available then they can also be considered as random variables to be inferred through the measurements[6]. This escalating approach leads to the so called *hierarchical models*. They are an interesting way of reducing the influence of the analyst, since the higher he/she injects information in the model, the lesser influence it has on the low placed random variables [34]. As a trade of, the number of random variables to infer increases, as well as the computational cost.

The choice of the prior PDF depends on the analyst and it is thus debatable. As such, it is often seen as a weak point of Bayesian methods due to the lack of a unique definition. In simple practical applications however, simple distributions conjugate to the likelihood are usually preferred in order to obtain a closed form of the conditional posterior PDFs of each random variable and so simplify the sampling algorithms. In this work, the same underlying choice has influenced the definition of the prior PDFs of the unknown random variables.

In the light of what said above, the estimation problem in Eq. (15) can be condensed through the hierarchical model in Fig. 8. The following assumptions have been made on the prior PDFs:

- The N_c components are a priori modelled as independent identically distributed stochastic processes, for which N_{bins} samples are available. Moreover, they are mutually independent, thus the prior PDF of the components reads:

$$[\hat{\mathcal{C}}|\boldsymbol{\theta}_{\hat{c}}] = \prod_{i=1}^{N_c} \prod_{s=1}^{N_{bins}} [\hat{c}_{i,s}|\theta_{\hat{c}}]\,, \tag{17}$$

  where $\boldsymbol{\theta}_{\hat{c}}$ stands for the set of parameters defining the prior distribution of the components. The choice of each prior distribution $[\hat{c}_{i,s}|\theta_{\hat{c}}]$ and corresponding parameters $\theta_{\hat{c}}$ determines the kind of factorial analysis performed. If, as in this work, an independent component analysis is wished then the prior distributions must not be Gaussian [31]. As a consequence, here Student t distributions are preferred, since they can be easily implemented in a Gibbs sampler by Scaled Mixture of Gaussian (SMOG) [33]. Under this assumption, the following prior PDFs are chosen for the components:

$$\begin{aligned} \forall i = 1,\dots,N_c,\ \forall s = 1,\dots,N_{bins} \quad & [\hat{c}_{i,s}|\hat{\mathfrak{c}}^J_{i,s}, \nu^2_{i,s}] \sim \mathcal{N}(\hat{\mathfrak{c}}^J_{i,s}, \nu^2_{i,s}) \\ & [\nu^2_{i,s}|\alpha_i, \beta_i] \sim \text{InvGamma}(\alpha_i, \beta_i)\,, \end{aligned} \tag{18}$$

  where the component prior mean $\hat{\mathfrak{c}}^J_{i,s}$ is fixed and chosen to be a prior estimation as yielded for instance by a deterministic ICA algorithm, while the variance $\nu^2_{i,s}$

[6] Then, they also need a prior PDF.

changes for each component i and torque/speed bin s as a random variable following an Inverse Gamma distribution (noted InvGamma). Fixing the prior to a good deterministic estimation (here by JADE algorithm [35]) is important to stabilise the SMOG algorithm that otherwise might have too many unknown random variables.

- The stability of the algorithm is also helped by favouring low values for the variances $\nu^2_{i,s}$, so that more weight is given to the prior estimation $\hat{c}^J_{i,s}$. To this aim, an exponential distribution is chosen for the parameters α_i:

$$\forall i = 1, \dots, N_c, \quad [\alpha_i | \mathrm{a}_\alpha] = \mathrm{a}_\alpha e^{-\mathrm{a}_\alpha \alpha_i}, \tag{19}$$

where the upright letter a_α stands for an hyper-parameter, i.e. a parameter which is not inferred but fixed by the analyst according to his/her knowledge. In this case, the parameter is high in the hierarchy, so that any non "degenerate" value is adapted and won't have much of an influence on the inference of the components distribution.

- Always to help the stability of the algorithm through low variance values, a Gamma distribution is chosen as prior for the parameters β_i:

$$\forall i = 1, \dots, N_c, \quad [\beta_i | \mathrm{a}_\beta, \mathrm{b}_\beta] \sim \mathrm{Gamma}(\mathrm{a}_\beta, \mathrm{b}_\beta), \tag{20}$$

where the terms a_β b_β are hyper-parameters chosen by the user, as before. Also note that the choice of a Gamma distribution is particularly adapted here since it is conjugate with respect to the Inverse Gamma distribution of the variances. This greatly simplifies the application of the Bayes theorem to retrieve the posterior distributions.

- The inference of the *pattern* matrix exploits all the N_{bins} samples (unlike the components, where a value for each sample has to be inferred). Therefore, enough information is available to perform a stable inference of the matrix $\hat{\Lambda}$ without the need for prior information. A non-informative prior can thus be chosen:

$$[\hat{\ell}_v] \sim 1, \tag{21}$$

with $\hat{\ell}_v = vec(\hat{\Lambda})$.

- The error variances appearing in Eq. (16) are supposed to follow an Inverse Gamma distribution as:

$$\forall j = 1, \dots, N_e, \quad \forall s = 1, \dots, N_{bins}, \quad [\sigma^2_{f_{j,s}} | \mathrm{a}_f, \mathrm{b}_f] = \mathrm{InvGamma}(\mathrm{a}_f, \mathrm{b}_f). \tag{22}$$

An Inverse Gamma distribution is adapted here since it is conjugate to the likelihood. As a consequence, it makes the posterior computation by Bayes theorem analytically feasible, while being flexible enough to convey the analyst knowledge (or lack of it).

Knowing the likelihood and the prior PDFs makes it possible to express the posterior PDF of the *patterns* $\hat{\Lambda}$, the components $\hat{C}$, and the error variances $\sigma^2_{f_{1,1}}, \dots, \sigma^2_{f_{N_e,N_{bins}}}$

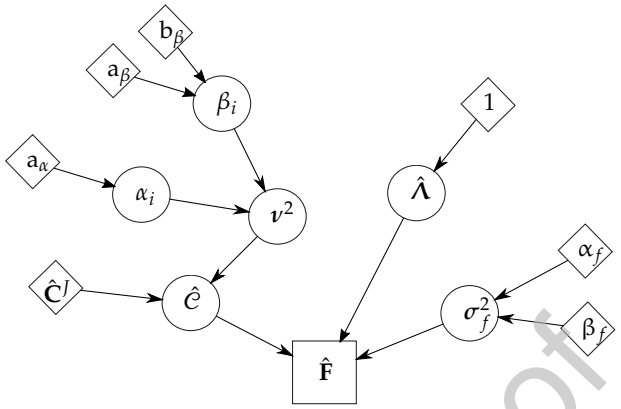

Figure 8: Hierarchical Bayesian model for ICA. Diamonds for hyper-parameters, rounds for parameters, squares for measurements. $\hat{\mathbf{F}}$ is the measurement set to be decomposed, $\hat{\mathcal{C}}$ stands for the independent components matrix to be inferred, $\nu^2 \in \mathbb{R}^{N_c \times N_{bins}}$ stands for the variances of the components, α_i and β_i are the parameters of the distribution of $\nu_i^2, \forall i = 1, \ldots, N_c$, $\hat{\mathbf{\Lambda}}$ is the *pattern* matrix, $\sigma_f^2 \in \mathbb{R}^{N_e \times N_{bins}}$ contains the variances of the noise $\hat{\mathcal{R}}$, $\hat{\mathbf{C}}^J$ is the estimation of the components made by JADE ICA used as hyper-parameter for $\hat{\mathcal{C}}$, the a and b in the diamonds are the others hyper-parameters chosen by the user.

in Eq. (15) (see Fig. 8 and Appendix B for the corresponding equations). In this work, the exploration of the posterior PDF is performed by means of Gibbs sampling [36]. Belonging to the MCMC methods, Gibbs sampling is an iterative algorithm that at each iteration yields a sample out of the posterior distribution of only one unknown random variable given all the others fixed at their most recent sampled value. After a number of iterations high enough, convergence toward the joint posterior distribution is ensured and can be for instance checked using the Gelman & Rubin convergence criterion [37]. Gibbs sampling is preferred here thanks to its fast convergence when it comes to hierarchical models [34]. Indeed, Knuth and Djafari [15, 16] showed that the decomposition in independent component can be formulated through a hierarchical model in the Bayesian framework. The algorithm is detailed in Appendix C.

One of the outputs of the algorithm is the posterior distribution of the component matrix $\hat{\mathcal{C}}$ described through its Gibbs samples as $\{\hat{\mathbf{C}}\} = \{\hat{\mathbf{C}}^{(1)}, \ldots, \hat{\mathbf{C}}^{(N_{run})}\}$ where N_{run} is the number of converged Gibbs iterations and $\forall r \in \{1, \ldots, N_{run}\}$, $\hat{\mathbf{C}}^{(r)} \in \mathbf{C}^{N_c \times N_{bins}}$ contains one sample of the evolution along the bins of the independent components. The other principal output is the posterior distribution of the mixing matrix $\hat{\mathbf{\Lambda}}$ described through its Gibbs samples as $\{\hat{\mathbf{\Lambda}}\} = \{\hat{\mathbf{\Lambda}}^{(1)}, \ldots, \hat{\mathbf{\Lambda}}^{(N_{run})}\}$ where $\forall r \in \{1, \ldots, N_{run}\}$, $\hat{\mathbf{\Lambda}}^{(r)} \in \mathbf{C}^{N_e \times N_c}$ contains the *patterns* corresponding to $\hat{\mathbf{C}}^{(r)}$.

If needed, any point estimate can be chosen out of the posterior distributions. For instance, the interpretations hereafter are performed using the mean as point estimate for the components and *patterns*.

3.1.5. *Interpreting the results: components vs. patterns*

Fig. 9 shows the relative contribution of each component to the acoustic level and it appears that ICA behaves as predicted: a sparse behaviour in the operating condi-

tions domain O is visible, since each component appears to be dominant in a different torque/speed region. This result has a remarkable engineering value when the components are analysed along the corresponding *patterns*, since each *pattern* condenses the behaviour of the excitation over the OC region highlighted by the component.

For instance, Fig. 10 shows in parallel the third component and its *pattern*. It appears to target the high torque scenario, while the pattern shows an important load component at the wheels along the X direction. Physically, this can be explained knowing that high torque scenarios imply high torque ripple at the wheels, which is in turn balanced by a load along the X direction at the wheel centre. Thus, not only the proposed approach finds a well known remarkable excitation *pattern* in a completely unsupervised way, but it also clearly defines the region of dominance of this excitation.

Another remarkable example is shown in Fig. 11, which shows the sixth component and its *pattern*. The component seems to target high engine speed scenarios, regardless of the torque. Usually in automotive engineering such a region is considered dominated by the pitch engine movement. Indeed, the pattern highlights a strong excitation at the right engine mount along the Z direction. As before, the proposed method allows a unique definition of the dominance region.

Finally, a definite advantage of the Bayesian formulation is to take into account the dispersion in each bin described in the structure $\{\tilde{\mathbf{F}}\}$. The posterior distributions of the mixing matrix $\hat{\boldsymbol{\Lambda}}$ as well as the components $\hat{\mathcal{C}}$ mirror the content of each torque/speed bin. For instance, Fig. 12 shows the acoustic level at the driver's ears along the active torque/speed bins. As it can be noticed, the dispersion of the recomposed level at the end of the probabilistic factor analysis (grey area) encompasses well the level recomposed directly from the loads $\mathbf{F}$ (red area), whose dispersion is only due to the presence of multiple occurrences inside the torque/speed bins. Note that the grey area in Fig. 12 mirrors not only the multiplicity of occurrences in a bin, but also the reduction and corresponding modelling error due to the choice of only N_c independent components.

3.2. Modelling the components

The analysis proposed in the previous section is already valuable as a standalone tool to understand the most common loading cases during the vehicle life and act on them if needed, by targeting only specific excitation DOFs. However, it becomes even more interesting in a modelling context since it separates DOFs-dependent *patterns* and OC-dependent components. As a consequence, to achieve a model of the loads, it is sufficient to model only the N_c components instead of modelling each of the N_e excitation DOFs. The modelled components are then multiplied by the *patterns* to obtain the loads.

The aim of this section is to present a modelling approach able to capture the evolution of the components with respect to the operating conditions and to propagate the dispersion described by the samples $\{\hat{\mathbf{C}}\}$ of the marginal posterior distribution of the components $\hat{\mathcal{C}}$. To do this, a Bayesian regression on a radial basis is proposed hereafter.

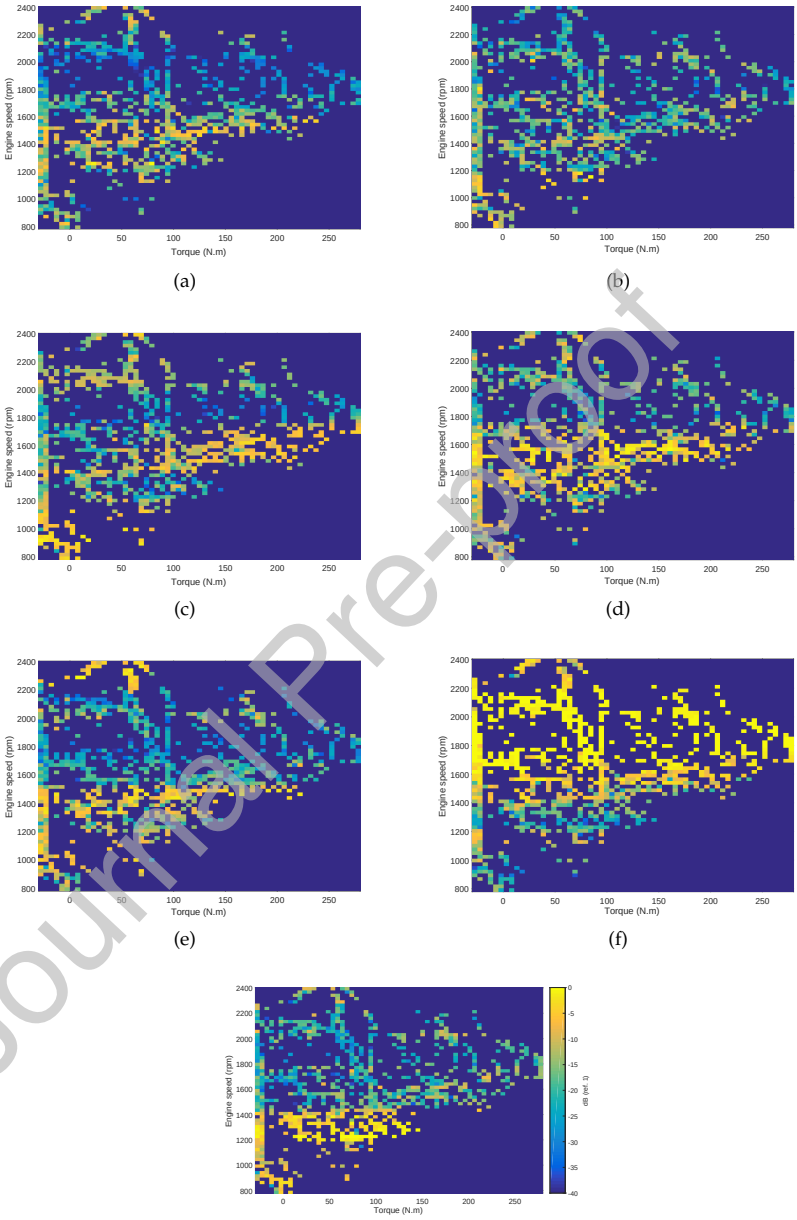

Figure 9: The relative contribution to the second harmonic h_2 of the acoustic level inside the car of $N_c = 7$ (a-g) extracted independent components with their evolution in the engine torque/speed plane.

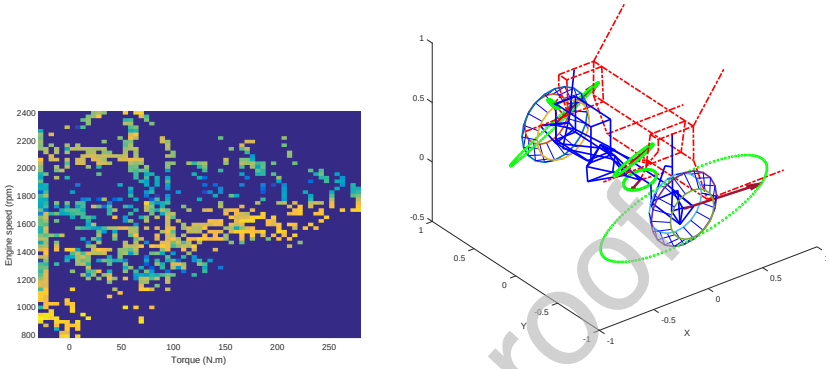

(a) (b)

Figure 10: (a) Relative contribution of component (c) in Fig. 9 to the acoustic level inside the car. (b) Corresponding *pattern*. The ellipses show the magnitude, while the arrows the phase relations among the excitation DOFs in a car.

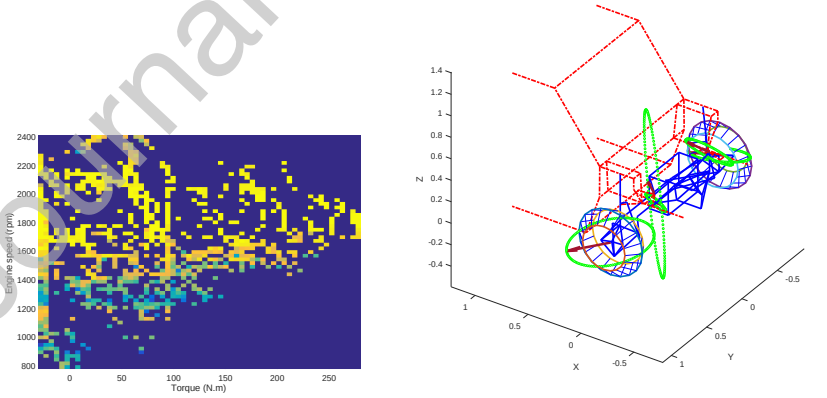

(a) (b)

Figure 11: (a) Relative contribution of component (f) in Fig. 9 to the acoustic level inside the car. (b) Corresponding *pattern*. The ellipses show the magnitude, while the arrows the phase relations among the excitation DOFs in a car.

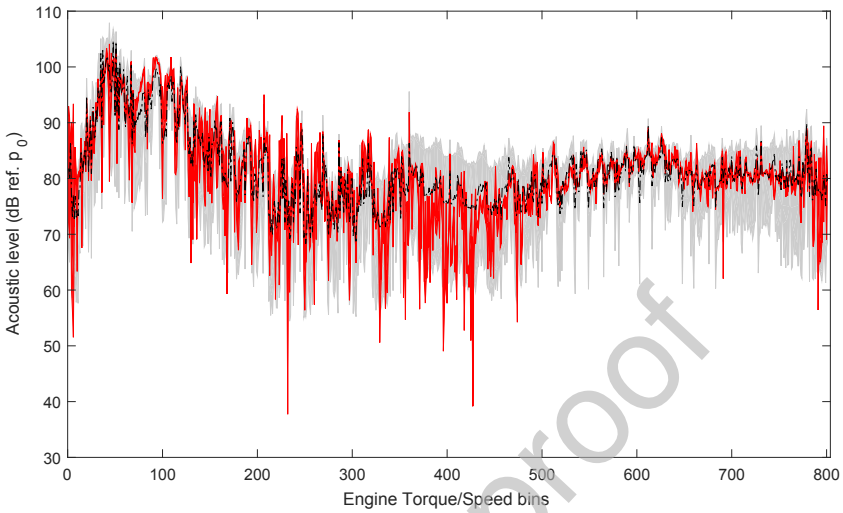

Figure 12: Acoustic level at the driver's ears (h_2 harmonic) along the active engine torque/speed bins. Comparison between the recomposition through the estimated loads **F** (red area) and the one obtained after reduction and analysis of the loads (grey area, black dashed median).

3.2.1. *Radial basis networks*

Let $\hat{\mathbf{C}} \in \mathbb{C}^{N_c \times N_{bins}}$ be a point estimator of the components $\hat{\mathcal{C}}$ (for instance the mean). Then two real matrices can be defined as:

$$\begin{aligned} \hat{\mathbf{C}}^{mod} &= \text{real}(\ln(\hat{\mathbf{C}})) \\ \hat{\mathbf{C}}^{ph} &= \text{imag}(\ln(\hat{\mathbf{C}}))\,, \end{aligned} \tag{23}$$

where $\hat{\mathbf{C}}^{mod} \in \mathbb{R}^{N_c \times N_{bins}}$ stores the natural logarithm of the components magnitude and $\hat{\mathbf{C}}^{ph} \in \mathbb{R}^{N_c \times N_{bins}}$ stores the phase. Then, finding a model for the complex components means finding one model for the magnitude and one for the phase. For both, the kind of model proposed is the same, so that for simplicity only the magnitude case is detailed.

Let $\hat{\mathcal{C}}^{mod}(r)$ be the continuous form of $\hat{\mathbf{C}}^{mod}$ in its evolution on the manifold $\mathbb{O}'$. The model chosen for $\hat{\mathcal{C}}^{mod}(r)$ reads:

$$\hat{\mathcal{C}}^{mod}(r) = \sum_{b=1}^{N_{rb}} \mathbf{w}_b \phi(||r - \mu_b||, \sigma_b^2)\,, \tag{24}$$

where $\phi(||r - \mu_b||, \sigma_b^2)$ is a radial basis function, i.e. a function symmetric with respect to a center μ_b and characterized by a spread σ_b^2. This kind of model is called *radial basis function* (RBF) model and it aims at decomposing the target as a sum of weighted (by weights $\mathbf{w}_b$) radial functions. It has been developed first in 1988 by Broomhead and Lowe [17] as a way of performing a simple non-linear modelling, which could approach

as precisely as desired a target function. Moreover, through the spread parameter, one can tune the regularization of the model, making this approach quite flexible [38].

The identification of a RBF model consists in finding the optimal number, position and spread of the radial functions (N_{rb}, μ_b and σ_b^2) and the weights $\mathbf{w}_b$ with respect to an arbitrary approximation goal and regularization coefficient chosen by the user. In the early days of machine computing, the identification was performed in a sequential way [39]: first an unsupervised step identified N_{rb}, μ_b and σ_b^2 in order to cover the manifold in the best way possible; then a simple regression between the target function and the computed basis yielded the weights $\mathbf{w}_b$. This simple although not optimal approach explains the early interest and wide use of this approach. Nowadays, it is inscribed in the appealing neural networks context, where it can be considered as a basic one hidden layer network. With the increased computational power at disposal, commercial software propose ready-to-use libraries to identify RBF models.

3.2.2. Bayesian take at RBF models

In this work, the RBF model is chosen as the simplest non-linear model. It is considered that linearity of the component magnitudes C^{mod} with respect to the OC is not realistic and a wider, but still easy to use model is adopted. Moreover, the model identification is inscribed in the Bayesian context. The approach proposed here is hybrid: the radial functions parameters (N_{rb}, μ_b and σ_b^2) are obtained by optimization using a commercial software, then the weight coefficients $\mathbf{w}_b$ are considered as random variables w_b, whose PDF is inferred by Bayesian regression.

As for the factor analysis, also regression problems can be tackled in a Bayesian framework. In the proposed application, the problem can be described as:

$$\hat{\mathcal{C}} = \mathcal{W}\mathbf{X} + \mathcal{E} \tag{25}$$

where a sample $\hat{\mathbf{C}}$ of the predicted random variable $\hat{\mathcal{C}} \in \mathbb{R}^{N_c \times N_{bins}}$ is available, as well as the measurement of the corresponding predictor variables $\mathbf{X} \in \mathbb{R}^{N_{rb} \times N_{bins}}$. The aim of the inference is the posterior distribution of the weights $\mathcal{W} \in \mathbb{R}^{N_c \times N_{rb}}$, their parameters and the error $\mathcal{E}$ variance.

Based on Eq. (25), the likelihood reads:

$$[\hat{\mathbf{c}}_v | \mathbf{X}, \mathcal{W}, \sigma^2_{c_{1,1}}, \dots, \sigma^2_{c_{N_c,N_{bins}}}] \sim \mathcal{N}\left(\hat{c}_v, \begin{bmatrix} \sigma^2_{c_{1,1}} & & \\ & \ddots & \\ & & \sigma^2_{c_{N_c,N_{bins}}} \end{bmatrix}\right), \tag{26}$$

where $\hat{\mathbf{c}}_v$ is a vectorization of $\hat{\mathcal{C}}$ while $\hat{c}_v$ a vectorization of product $\mathcal{W}\mathbf{X}$. Moreover, note that the variance is supposed to change for each engine torque/speed bin, making this kind of regression a SMOG model [8, 33].

As before, in order to use the Bayes theorem, some prior distributions have to be defined. In this case of application, the hierarchical model is shown in Fig. 13 and the following choices have been made for the prior PDFs:

- The modelling error variances are supposed to be different for each component and for each engine torque/speed bin. They are also supposed to follow an Inverse Gamma PDF as:

$$\forall i = 1, \dots, N_c, \quad \forall s = 1, \dots, N_{bins}, \quad [\sigma^2_{c_{i,s}} | \alpha_c, \beta_c] \sim \text{InvGamma}(\alpha_c, \beta_c)\,. \tag{27}$$

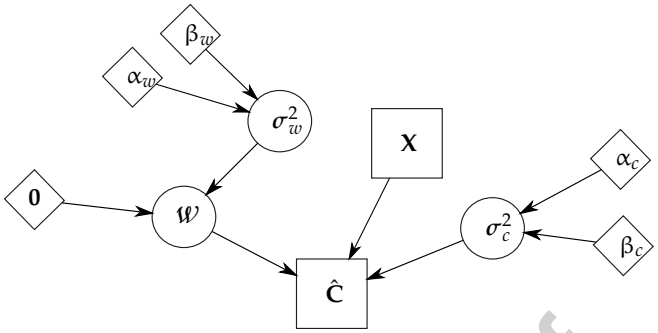

Figure 13: Hierarchical Bayesian model for the regression. Diamonds for hyper-parameters, rounds for parameters, squares for measurements. $\hat{\mathbf{C}}$ is the predicted variable sample, while $\mathbf{X}$ stands for the predictor variables sample. $\mathcal{W}$ is the weight matrix to infer, whose prior mean is 0 and variance $\sigma_w^2 \in \mathbb{R}^{N_c \times N_{rb}}$. The hyper-parameters of σ_w^2 are chosen by the user and noted α_w and β_w. $\sigma_c^2 \in \mathbb{R}^{N_c \times N_{bins}}$ contains the variances of the error $\mathcal{E}$, which are supposed to follow Inverse Gamma distributions of hyper-parameters α_c and β_c.

The choice for the Inverse Gamma PDF is dictated by practicality. The terms α_c and β_c are hyper-parameters chosen by the analyst.

- The weights are supposed to follow a Gaussian PDF as:

$$[w_v|\sigma^2_{w_{1,1}}, \dots, \sigma^2_{w_{N_c,N_{rb}}}] \sim \mathcal{N}\left(0, \begin{bmatrix} \sigma^2_{w_{1,1}} & & \\ & \ddots & \\ & & \sigma^2_{w_{N_c,N_{rb}}} \end{bmatrix}\right) \tag{28}$$
$$\forall i = 1, \dots, N_c, \quad \forall b = 1, \dots, N_{rb}, \quad [\sigma^2_{w_{i,b}}|\alpha_w, \beta_w] \sim \text{InvGamma}(\alpha_w, \beta_w)\,,$$

where w_v is a vectorization of matrix $\mathcal{W}$.

Note that a null prior mean is supposed here in order to help the sparsity of the model. Otherwise, the choice of the Gaussian PDF (and Inverse Gamma PDF for the variances) is dictated by practicality to lead to a fast and stable sampling algorithm.

Having defined the likelihood and the prior distributions, again Gibbs sampling can be used to obtain a collection of samples out of the target posterior distribution. The algorithm is detailed in Appendix D. The posterior computations leading to the algorithm are very similar if not simpler than those in Appendix B, therefore they are not detailed in this work.

The Bayesian approach is here necessary to propagate the dispersion of $\hat{\mathcal{C}}$ described by all the samples $\{\hat{\mathbf{C}}\}$. Indeed, instead of using $\hat{\mathbf{C}}^{mod}$ as input data, at each iteration of the Gibbs sampler one single occurrence of the components is randomly drawn following a uniform distribution out of the population $\{\hat{\mathbf{C}}\}$. After a number high enough of iterations, the measurement space described by $\{\hat{\mathbf{C}}\}$ will have been visited and the posterior distribution of the weights $\mathcal{W}$ will mirror the component dispersion. For instance, Fig. 14 compares the population of the sixth component magnitude to the RBF model

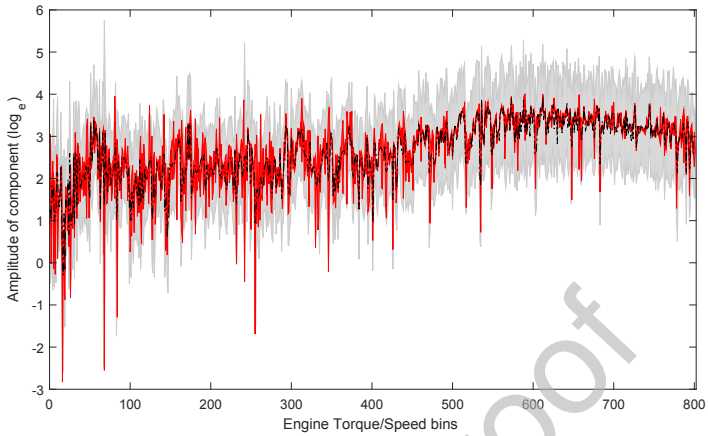

Figure 14: Magnitude of the sixth component along the active engine torque/speed bins (in natural logarithmic scale). Comparison between the population in $\{\hat{\mathbf{C}}\}$ (red area) and the one simulated through the RBF model (grey area, black dashed mean).

prediction. It can be noticed that the prediction encompasses the input samples, with a dispersion that is increased since it also mirrors the modelling error.

The same approach can be applied to the components phase whose point estimator has been previously noted $\hat{\mathbf{C}}^{ph}$. Fig. 15 compares the population of the sixth component phase to the RBF model prediction. As it can be seen, the 95% credible interval of the prediction is often larger than 2π. This implies a phase virtually unpredictable as a function of the operating conditions[7]. As a consequence, the choice has been made to focus on and model only the magnitude of the components. When synthesizing and predicting the loads and the acoustic level as a function of the operating conditions, a random phase is assigned to the components, while keeping all phase relations in the *patterns* and FRFs. The effects of such an assumption on the acoustic level prediction are pointed out in the next section.

At this point, the wished useful reduced model for the loads has been built. From an operating condition input, the components can be simulated, then they are multiplied by the OC-independent *patterns* and FRFs in order to obtain a prediction of the response of the vehicle. To give more details about this synthesis process and verify its feasibility is the aim of the next section.

4. Model exploitation

4.1. Discussion on the obtained meta-model

The processing in the previous sections reduces the identified loads $\mathbf{F}$ to $\tilde{\mathbf{F}}$ choosing wisely the components, then applies a change of variable to $\tilde{\mathbf{F}}$ in order to analyse it in the

[7] With this kind of model and component dispersion.

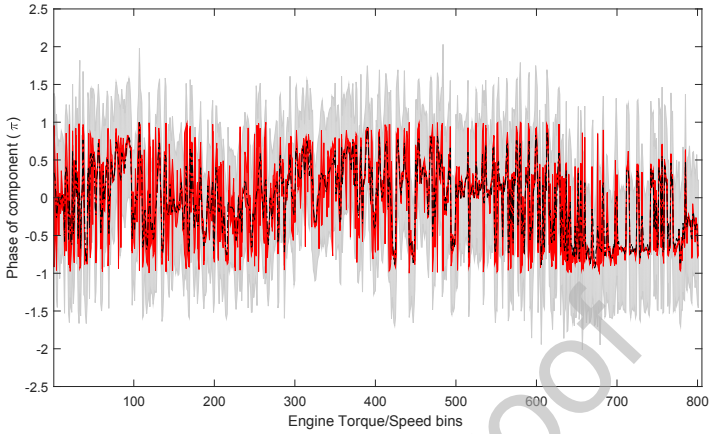

Figure 15: Phase of the sixth component along the active engine torque/speed bins. Comparison between the population in $\{\hat{\mathbf{C}}\}$ (red area) and the one simulated through the RBF model (grey area, black dashed mean).

engine torque/speed plane. This leads to the structure $\{\tilde{\mathbf{F}}\}$ that stores all the reduced load samples in torque/speed bins. Afterwards, a modified Bayesian ICA is performed and the marginal posterior distributions for the components $\hat{C}$ and for the patterns $\hat{\mathbf{\Lambda}}$ are obtained. Finally, the components are modelled as a function of the OCs.

Note that none of the previous steps is truly "reversible":

- The data reduction by definition trades a decreased dimension of the data description for the appearance of a random error. The statistical properties of the error can be inferred, but the exact reconstruction of the input signal is impossible. Normally this is completely accepted since the measured data itself is polluted by noise, so that a good reduction processing is supposed to keep the fundamental characteristics of the input and to interpret the rest as noise. Thus, it reduces the data weight and also delivers a "clean" version of the signal.
- The change of variable, due to the absence of a bijective map, prevents a signal in the torque/speed-domain to be changed back to the exact previous signal in the time-domain. Once multiple time samples are put in the same torque/speed bin, the time information is not kept and the exact time at which a sample has been measured cannot be traced back.
- The Bayesian ICA does not process all the samples in one single bin one by one, but at each iteration draws randomly one sample. The correspondence between the samples in the bins and the iterations at which they have been drawn is not available and it is not of interest. The information that is propagated by the Bayesian algorithm is only the dispersion inside each bin.
- Modelling the components as a function of the operating conditions yields an approximate simulation, whose error is known and can be propagated. Moreover, as shown previously, this error prevents the model on the phase to be useful.

Therefore, only the magnitude of the independent components is modelled. These losses of information prevent the exact components to be retrieved.

This being said, the proposed model has not the ambition of recomposing the exact acoustic level measured inside the cabin, but it is more intended to provide an overall broad prediction of the noise level with a well determined credible interval, which accounts for all loss of information in the modelling process.

4.2. Synthesis steps

The forward synthesis steps are, thus, the following:

1. Simulate a sample of the operating conditions $\mathbf{O}$ following a target client profile[8]. One simple way of doing this is to use *slice* sampling [40].
2. Use the Bayesian regression model to obtain the components magnitude from the operating conditions. When simulating the components a Monte Carlo approach can be performed to propagate the uncertainty in the model identification to the components. Then, a random phase is considered for the amplitudes to get a sample $\{\hat{\mathbf{C}}\}^{(synth)}$ of components related to the input OCs.
3. The components are multiplied by the *patterns* to yield the loads. By Monte Carlo, random samples out of $\{\hat{\mathbf{C}}\}^{(synth)}$ are multiplied by random samples out of $\{\hat{\mathbf{\Lambda}}\}$ to yield samples of the harmonic loads $\{\mathbf{F}\}^{(synth)}$.
4. The loads are multiplied by the transfer function $\mathbf{H}$. If the latter are considered as deterministic, then every sample in $\{\mathbf{F}\}^{(synth)}$ is simply multiplied by the FRFs and a population of the vehicle response level $\{\mathbf{U}\}^{(synth)}$ is obtained. If they are stochastic - obtained for instance by a non-parametric stochastic finite element approach - and described by a set of samples $\{\mathbf{H}\}$, again Monte Carlo techniques can be used to propagate both the dispersion of the FRFs and the loads to $\{\mathbf{U}\}^{(synth)}$.
5. $\{\mathbf{U}\}^{(synth)}$ is the population of the vehicle response representative of the client profile and of the loads and FRFs uncertainty. From these samples any statistical analysis can be performed.

Remark that important approximations are made in steps 2 and 3. In step 2, an arbitrary random phase is applied to the component amplitudes. Note that out of the Bayesian ICA step the components have a defined phase, however resorting to a random phase is justified in the following modelling step by the need of a simple model to be used industrially: such a simple model is not able to simulate the evolution of the component phases. This may seem an important limitation specific to this work, but it is in fact quite common. For instance, in the mid-high frequency domain the phase is very hard to analyse and one is in practice led to focus only on the magnitude. This work targets a lower frequency band, but, as it will be shown in the application, assuming a random phase for the components still does not sensibly worsen the load synthesis.

[8] In the automotive industry, usually client profiles are described through a joint distribution of the most important driving parameters (such as engine torque and speed and vehicle speed).

In step 3, the modelled components are multiplied by the *patterns* and a Monte Carlo approach is proposed as a way of propagating the uncertainty described in $\{\hat{\mathbf{C}}\}^{(synth)}$ and $\{\hat{\mathbf{\Lambda}}\}$. Note that this approach assumes the components $\hat{\mathcal{C}}^{(synth)}$ and the *patterns* $\hat{\mathbf{\Lambda}}$ to be independent. Out of the Bayesian ICA step, this is clearly not the case: they are classically defined by their joint posterior distribution[9]. However, the simulated components $\{\hat{\mathbf{C}}\}^{(synth)}$ come from a RBF modelling of the components amplitude with a random phase, therefore any kind of dependence with respect to the *pattern* samples is assumed lost. The effects of these assumptions are pointed out in the application below.

4.3. Application

To validate the meta-model, the measured acoustic level at the driver's ear during the driving test is recomposed using the identified model. Fig. 17 shows the comparison between the measurement and the simulation for each modelling step. It must be noted that in Figs. 17(b-c) the measurement and the model are not in the same domain. The measurement is in the time domain, whereas the simulation comes from components defined on the engine torque/speed space. However, since the time trajectory of the operating conditions is known (in matrix $\mathbf{O}$), the torque/speed bin visited at each time can be obtained and thus the simulation plotted in the time domain.

More in general, it is clear that the further one goes with the model the more the uncertainty increases. This is well testified through the credible intervals, here unilateral upper 95% credible intervals[10]. Fig. 18 compares specifically the noise level prediction achieved after the Bayesian ICA, keeping the phase of the components (green lines) or using a random phase (blue lines). It is interesting to notice that the performance of the mean prediction is globally unchanged, as well as the credible interval which widens just locally to mirror the loss of information.

Finally, a scalar indicator can be used to condense the information of the prediction and convey an idea of the vehicle performance. The indicator proposed here is the equivalent noise level, defined as:

$$\mathbf{L}_{h_o,eq} = 10 \cdot \log_{10}\left(\frac{1}{N}\sum_{n=1}^{N}\frac{|\mathbf{p}_{h_o,n}|^2}{p_0^2}\right), \tag{29}$$

where $\mathbf{p}_{h_o,n} \in \mathbb{C}^{N_o}$ is the n^{th} time sample of the h_o harmonic acoustic pressure at the N_o microphones inside the cabin (measured or simulated).

Moreover, as a whole population of acoustic levels can be simulated from the input OCs, the same can be done for a population of indicators $\{\mathbf{L}_{h_o,eq}\}$. This allows the median equivalent level prediction as well as the inherent credible intervals to be computed. Table 2 resumes the equivalent level measurement and predictions at four microphones inside the vehicle for the second harmonic in the real driving test.

[9] Which is different from the product of their marginal posterior distributions. Behaviour that is implied by the independence.

[10] In engineering applications one is more concerned with the upper limit of a prediction since it may cause problems with respect to the clients perception of quality.

	Measured $\mathbf{L}_{h_2,eq}$ (dB ref. p_0)	Simulated $\mathbf{L}_{h_2,eq}$ (dB ref. p_0)	
		Median	Upper 95% credible interval
Rear right	86.78	86.85	95.15
Rear left	87.03	87.69	95.99
Front right	86.82	88.04	96.79
Front left	85.87	87.82	96.55

Table 2: The equivalent level $\mathbf{L}_{h_2,eq}$ at the 4 microphones inside the vehicle cabin: measured and simulated by the model.

It can be noticed that the gap between the median predicted level and the measured one is acceptably low (maximum 2 dB), which means that the median is a pertinent point estimate. However, as expected the wide credible intervals testify for the several simplifications adopted in the model identification. If a more precise model is searched, one can skip some of the steps that introduce uncertainties (such as the reduction) and/or use a more advanced way of modelling the components.

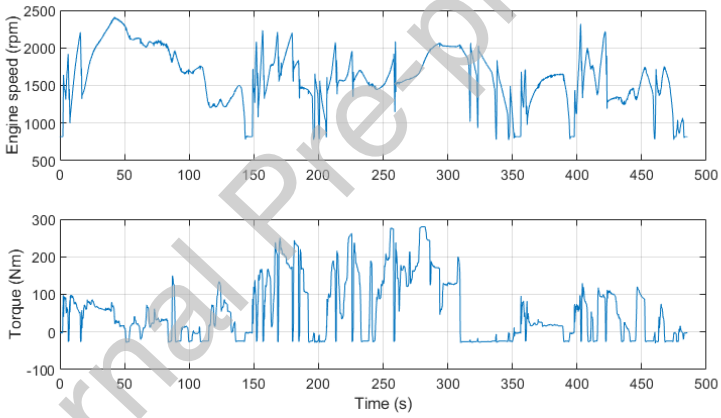

Figure 16: Engine speed and torque corresponding to the loads processed in this paper.

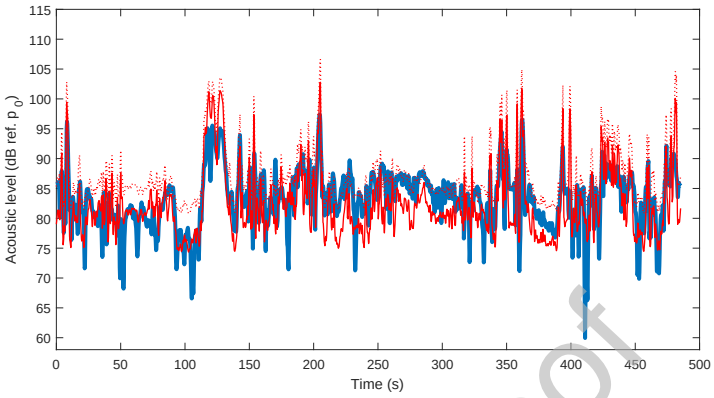

(a)

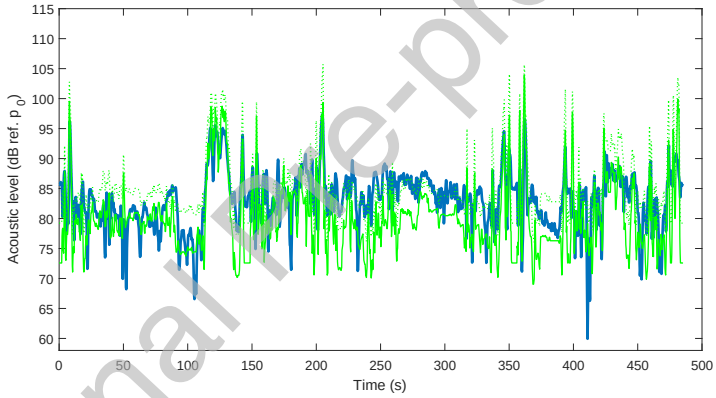

(b)

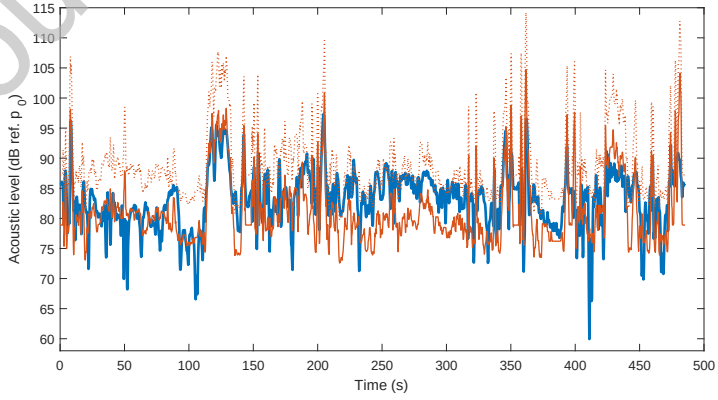

(c)

Figure 17: Acoustic level (h_2 harmonic) inside the car at the driver's ears. In solid blue line the measured level. In red (a) the recomposition through the identified loads, in green (b) the recomposition through the independent components and in brown (c) the recomposition through the radial basis model of the components. In the three figures the median is in solid line and the 95% upper credible interval in dotted line. The curves are smoothed over 1 s.

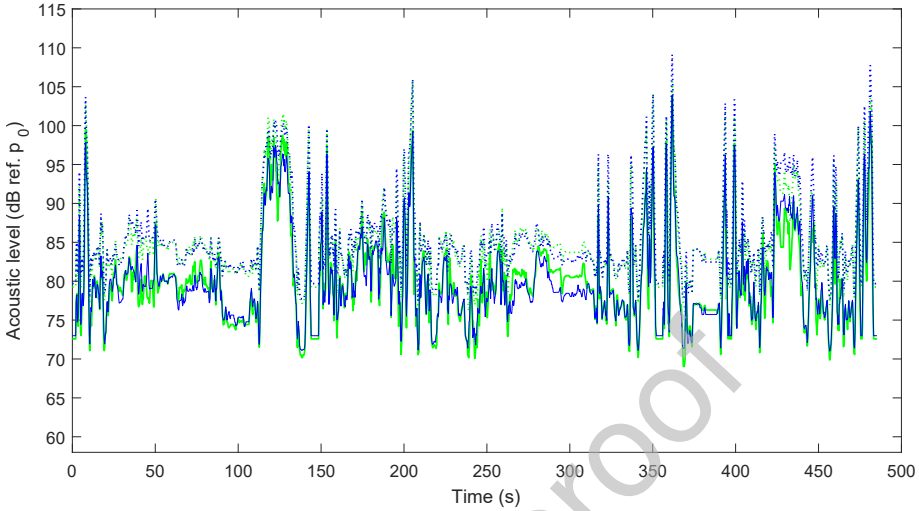

Figure 18: Acoustic level (h_2 harmonic) at the driver's ear. Comparison between the recomposition through the components magnitude and phase (in green) and the one through the components magnitude and a random phase (in dark blue). The medians are in solid line and the 95% upper credible intervals in dotted line. The curves are smoothed over 1 s.

5. Conclusion

In order to achieve the prediction of booming noise performance, this paper introduced a meta-model of the harmonic excitation sources in a vehicle. Unlike what is proposed in the literature to the authors knowledge, the proposed approach has the advantage to cover most of the vehicle usage conditions. This means that the acoustic quality can now be judged looking at entire client profiles, rather than only at "extreme" scenarios. This will allow a better optimised vehicle design leading to a reduction of production cost and/or an increased comfort for the drivers and passengers.

To build such a meta-model, Independent Component Analysis has been chosen as way to perform data reduction. Of all possible approaches, ICA has the peculiarity of yielding sparse components. This property has been used to achieve the complementary (but nonetheless interesting) result of defining excitation *patterns* specific to OC regions. These *patterns* have been demonstrated to be useful for acoustic validation in automotive industry.

Besides, reduction and modelling approaches intrinsically imply modelling errors. In order to understand, infer and propagate such errors in the meta-model, each algorithm has been developed in the Bayesian framework. Even if it may seem that this choice increases the complexity, the authors believe that the Bayesian framework is the most suited to aforementioned tasks, making it finally the "simplest" approach.

Finally, the meta-model can be extended to account for wide-band excitations and, thus, open to an even larger scope of applications, ranging from vehicle rolling noise to, for instance, drones vibration. More generally, the main aim of the model is to target systems whose operating conditions are spread, nonstationary, and uncontrolled.

Acknowledgement(s)

This work was funded by Stellantis N.V. and performed within the framework of the OpenLab Vibro-Acoustic-Tribology@Lyon and the LabEx CeLyA of Université de Lyon, operated by the French National Research Agency (ANR-10-LABX-0060/ANR-11-IDEX-0007).

Appendix A. Usual PDFs

Appendix A.1. Multivariate real normal distribution

The multivariate normal distribution of a N-dimensional random vector $\boldsymbol{x} \in \mathbb{R}^{N\times 1}$ is noted:

$$[\boldsymbol{x}] \sim \mathcal{N}(\boldsymbol{\mu}, \boldsymbol{\Sigma}) \,, \tag{A.1}$$

where $\boldsymbol{\mu}$ is the N-dimensional mean vector

$$\boldsymbol{\mu} = \mathbb{E}\{\mathbf{x}\} \tag{A.2}$$

and $\boldsymbol{\Sigma}$ is the $N \times N$ covariance matrix

$$\boldsymbol{\Sigma} = \mathbb{E}\{(\boldsymbol{x} - \boldsymbol{\mu})(\boldsymbol{x} - \mu)^t\} \,, \tag{A.3}$$

with $\mathbb{E}\{\bullet\}$ the expected value operator and $\bullet^t$ the transpose operator.
In the non-degenerate case (i.e. $\boldsymbol{\Sigma}$ is definite positive), the PDF of the multivariate real normal distribution is written:

$$[\boldsymbol{x}|\boldsymbol{\mu}, \boldsymbol{\Sigma}] = \frac{1}{(2\pi)^{N/2}\det^{\frac{1}{2}}\boldsymbol{\Sigma}} e^{-\frac{1}{2}(\mathbf{x}-\boldsymbol{\mu})^t\boldsymbol{\Sigma}^{-1}(\mathbf{x}-\boldsymbol{\mu})} \,, \tag{A.4}$$

where $\det \bullet$ stand for the determinant of a matrix.

Appendix A.2. Gamma distribution

The Gamma distribution can be parametrized using the shape parameter α and the rate parameter β. A random variable x which follows a Gamma distribution is noted:

$$[x] \sim \text{Gamma}(\alpha, \beta) \,. \tag{A.5}$$

The corresponding PDF is written as:

$$[x|\alpha, \beta] = \frac{\beta^{\alpha}}{\Gamma(\alpha)} x^{\alpha-1} e^{-\beta x} \,, \tag{A.6}$$

where $\Gamma(\bullet)$ stands for the Gamma function. Its support is $\mathbb{R}^+$.

Appendix A.3. Inverse-Gamma distribution

The Inverse-Gamma distribution can be parametrized using the shape parameter α and the rate parameter β. A random variable x which follows an Inverse-Gamma distribution is noted:

$$[x] \sim \text{InvGamma}(\alpha, \beta) \,. \tag{A.7}$$

The corresponding PDF is written as:

$$[x|\alpha, \beta] = \frac{\beta^{\alpha}}{\Gamma(\alpha)} x^{-\alpha-1} e^{-\frac{\beta}{x}} \,. \tag{A.8}$$

Its support is $\mathbb{R}^+$. If $[x] \sim \text{Gamma}(\alpha, \beta)$ then $[1/x] \sim \text{InvGamma}(\alpha, \beta)$.

Appendix A.4. Exponential distribution

The exponential distribution is parametrized using a rate parameter λ. A random variable x which follows an Exponential distribution is noted:

$$[x] \sim \text{Exp}(\lambda)\,. \tag{A.9}$$

The corresponding PDF is written as:

$$[x|\lambda] = \begin{cases} \lambda e^{-\lambda x}, & x \geq 0 \\ 0, & x < 0 \end{cases}. \tag{A.10}$$

Its support is $\mathbb{R}^+$. If $[x] \sim \text{Exp}(\lambda)$ then $[x] \sim \text{Gamma}(1, \lambda)$.

Appendix A.5. Multivariate complex normal distribution

If the complex normal random vector $\boldsymbol{x}$ is improper, than the PDF is written:

$$[\boldsymbol{x}|\breve{\boldsymbol{\mu}}_x, \breve{\boldsymbol{\Sigma}}_{xx}] = \frac{1}{\pi^n \det^{\frac{1}{2}} \breve{\boldsymbol{\Sigma}}_{xx}} \exp\left\{-\frac{1}{2}(\breve{\mathbf{x}} - \breve{\boldsymbol{\mu}}_x)^H \breve{\boldsymbol{\Sigma}}_{xx}^{-1} (\breve{\mathbf{x}} - \breve{\boldsymbol{\mu}}_x)\right\}, \tag{A.11}$$

where the breve mark stands for the *augmented* versions the random variable $\breve{\boldsymbol{x}}$, the mean $\breve{\boldsymbol{\mu}}$ and the covariance $\breve{\boldsymbol{\Sigma}}_{xx}$.
If the complex normal random vector $\boldsymbol{x}$ is proper, than the PDF is written:

$$[\boldsymbol{x}|\boldsymbol{\mu}_x, \boldsymbol{\Sigma}_{xx}] = \frac{1}{\pi^n \det \boldsymbol{\Sigma}_{xx}} \exp\left\{-(\mathbf{x} - \boldsymbol{\mu}_x)^H \boldsymbol{\Sigma}_{xx}^{-1} (\mathbf{x} - \boldsymbol{\mu}_x)\right\}, \tag{A.12}$$

where $\boldsymbol{\mu}_x$ and $\boldsymbol{\Sigma}_{xx}$ are respectively the mean and the covariance of $\boldsymbol{x}$.

Appendix B. Posterior PDF computation

In what follows, the details about the computation of the Bayesian posterior distributions for the Bayesian Independent Component Analysis are proposed.

The posterior PDFs at the r^{th} iteration of the Gibbs sampling algorithm are obtained as follows:

- Posterior distribution of $\sigma^2_{f_{j,s}}$, $\forall j \in [1, \ldots, N_e]$, $\forall s \in [1, \ldots, N_{bins}]$:

$$\begin{aligned} \text{Likelihood}: \quad & [\hat{\mathrm{f}}_{j,s}|\hat{\boldsymbol{\ell}}_j, \hat{c}_s, \sigma^2_{f_{j,s}}] \sim \mathcal{N}(\hat{\boldsymbol{\ell}}_j \hat{c}_s, \sigma^2_{f_{j,s}})\,. \\ \text{Prior}: \quad & [\sigma^2_{f_{j,s}}] \sim \text{InvGamma}(\alpha_f, \beta_f)\,. \end{aligned} \tag{B.1}$$

$$
\begin{aligned}
[\sigma^2_{f_{j,s}}|\text{rest}] &\propto [\hat{\mathrm{f}}_{j,s}|\hat{\mathbf{l}}_j^{(r-1)}, \hat{\mathbf{c}}_s^{(r-1)}, \sigma^2_{f_{j,s}}][\sigma^2_{f_{j,s}}] \\
&\propto \mathcal{N}(\hat{\mathbf{l}}_j^{(r-1)}\hat{\mathbf{c}}_s^{(r-1)}, \sigma^2_{f_{j,s}}) \cdot \text{InvGamma}(\alpha_f, \beta_f) \\
&\propto \frac{1}{\pi\sigma^2_{f_{j,s}}} \exp\left(-\frac{1}{\sigma^2_{f_{j,s}}}(\hat{\mathrm{f}}_{j,s} - \hat{\mathbf{l}}_j^{(r-1)}\hat{\mathbf{c}}_s^{(r-1)})^H(\hat{\mathrm{f}}_{j,s} - \hat{\mathbf{l}}_j^{(r-1)}\hat{\mathbf{c}}_s^{(r-1)})\right) \cdots \\
&\times \frac{\beta_f^{\alpha_f}}{\Gamma(\alpha_f)}(\sigma^2_{f_{j,s}})^{-\alpha_f-1} e^{-\frac{\beta_f}{\sigma^2_{f_{j,s}}}} \\
&\propto (\sigma^2_{f_{j,s}})^{-\alpha_f-2} \exp\left(-\frac{1}{\sigma^2_{f_{j,s}}}\left((\hat{\mathrm{f}}_{j,s} - \hat{\mathbf{l}}_j^{(r-1)}\hat{\mathbf{c}}_s^{(r-1)})^H(\hat{\mathrm{f}}_{j,s} - \hat{\mathbf{l}}_j^{(r-1)}\hat{\mathbf{c}}_s^{(r-1)}) + \beta_f\right)\right),
\end{aligned}
$$

Note that in Eq. (B.2) the only random term is the variance $\sigma^2_{f_{j,s}}$. In particular, the equation is identified to be an Inverse-Gamma distribution with parameters $\alpha'_f = \alpha_f + 1$ and $\beta'_f = (\hat{\mathrm{f}}_{j,s} - \hat{\mathbf{l}}_j^{(r-1)}\hat{\mathbf{c}}_s^{(r-1)})^H(\hat{\mathrm{f}}_{j,s} - \hat{\mathbf{l}}_j^{(r-1)}\hat{\mathbf{c}}_s^{(r-1)}) + \beta_f$.

- Posterior distribution of $\hat{\boldsymbol{\ell}}_j^t$, $\forall j \in [1, \ldots, N_e]$:

$$
\begin{aligned}
\text{Likelihood}: \quad & [\hat{\mathbf{f}}_j^t|\hat{\boldsymbol{\ell}}_j^t, \hat{\mathcal{C}}, \sigma^2_{f_{j,1}}, \ldots, \sigma^2_{f_{j,N_{bins}}}] \sim \mathcal{N}((\hat{\boldsymbol{\ell}}_j\hat{\mathcal{C}})^t, \boldsymbol{\Sigma}_f)\,. \\
\text{Prior}: \quad & [\hat{\boldsymbol{\ell}}_j] \propto 1\,.
\end{aligned}
\tag{B.2}
$$

$$
\begin{aligned}
[\hat{\boldsymbol{\ell}}_j^t|\text{rest}] &\propto [\hat{\mathbf{f}}_j^t|\hat{\boldsymbol{\ell}}_j^t, \hat{\mathbf{C}}^{(r-1)}, \boldsymbol{\Sigma}_f] \\
&\propto \mathcal{N}((\hat{\boldsymbol{\ell}}_j\hat{\mathcal{C}})^t, \boldsymbol{\Sigma}_f) \\
&\propto \frac{1}{\pi^{N_{bins}}\det(\boldsymbol{\Sigma}_f)} \exp\left(-(\hat{\mathbf{f}}_j^t - (\hat{\boldsymbol{\ell}}_j\hat{\mathbf{C}}^{(r-1)})^t)^H\boldsymbol{\Sigma}_f^{-1}(\hat{\mathbf{f}}_j^t - (\hat{\boldsymbol{\ell}}_j\hat{\mathbf{C}}^{(r-1)})^t)\right) \\
&\propto \exp\left((-\hat{\boldsymbol{\ell}}_j^*\hat{\mathbf{C}}^{(r-1)\,*}\boldsymbol{\Sigma}_f^{-1}\hat{\mathbf{C}}^{(r-1)\,t}\hat{\boldsymbol{\ell}}_j^t + \hat{\mathbf{f}}_j^*\boldsymbol{\Sigma}_f^{-1}\hat{\mathbf{C}}^{(r-1)\,t}\hat{\boldsymbol{\ell}}_j^t + \hat{\boldsymbol{\ell}}_j^*\hat{\mathbf{C}}^{(r-1)\,*}\boldsymbol{\Sigma}_f^{-1}\hat{\mathbf{f}}_j^t)\right).
\end{aligned}
\tag{B.3}
$$

A Multivariate Gaussian distribution for a random variable $\boldsymbol{x}^t$ with mean $\mathbf{m}$ and covariance matrix $\mathbf{S}$ would lead to:

$$
[\boldsymbol{x}^t|\mathbf{m}, \mathbf{S}] \propto \exp\left(-\boldsymbol{x}^*\mathbf{S}^{-1}\boldsymbol{x}^t + \boldsymbol{x}^*\mathbf{S}^{-1}\mathbf{m} + \mathbf{m}^H\mathbf{S}^{-1}\boldsymbol{x}^t\right). \tag{B.4}
$$

Eqs. (B.3) and (B.4) have the same form and by identification it can be recognised that the posterior distribution of $\hat{\boldsymbol{\ell}}_j^t$ is a Multivariate Gaussian distribution with parameters:

$$
\begin{aligned}
\boldsymbol{\mu}_{l_j} &= \boldsymbol{\Sigma}_{l_j}\hat{\mathbf{C}}^{(r-1)\,*}\boldsymbol{\Sigma}_f^{-1}\hat{\mathbf{f}}_j^t \\
\boldsymbol{\Sigma}_{l_j}^{-1} &= (\hat{\mathbf{C}}^{(r-1)}\boldsymbol{\Sigma}_f^{-1}\hat{\mathbf{C}}^{(r-1)\,H})^*\,.
\end{aligned}
\tag{B.5}
$$

It is reminded that has defined in the algorithm, here $\boldsymbol{\Sigma}_f = \text{diag}(\sigma^{2\,(r)}_{f_{j,1}}, \ldots, \sigma^{2\,(r)}_{f_{j,N_{bins}}})$.

- To prove the posterior PDF computation of $\hat{c}_{i,s}$, the model in Eq. (15) has to be rewritten for all $s \in \{1, \dots, N_{bins}\}$ as:

$$\begin{aligned} \hat{\mathbf{f}}_s &= \hat{c}_{i,s}\hat{\boldsymbol{\lambda}}_i + \sum_{k \neq i} \hat{c}_{k,s}\hat{\boldsymbol{\lambda}}_k + \mathbf{r}_s \\ \frac{\hat{\boldsymbol{\lambda}}_i^H \hat{\mathbf{f}}_s}{\hat{\boldsymbol{\lambda}}_i^H \hat{\boldsymbol{\lambda}}_i} &= \hat{c}_{i,s} + \sum_{k \neq i} \hat{c}_{k,s} \frac{\hat{\boldsymbol{\lambda}}_i^H \hat{\boldsymbol{\lambda}}_k}{\hat{\boldsymbol{\lambda}}_i^H \hat{\boldsymbol{\lambda}}_i} \hat{c}_{k,s} + \frac{\hat{\boldsymbol{\lambda}}_i^H \mathbf{r}_s}{\hat{\boldsymbol{\lambda}}_i{}^H \hat{\boldsymbol{\lambda}}_i} \\ \frac{\hat{\boldsymbol{\lambda}}_i^H \hat{\mathbf{f}}_s}{\hat{\boldsymbol{\lambda}}_i^H \hat{\boldsymbol{\lambda}}_i} - \sum_{k \neq i} \hat{c}_{k,s} \frac{\hat{\boldsymbol{\lambda}}_i^H \hat{\boldsymbol{\lambda}}_k}{\hat{\boldsymbol{\lambda}}_i^H \hat{\boldsymbol{\lambda}}_i} \hat{c}_{k,s} &= \hat{c}_{i,s} + \frac{\hat{\boldsymbol{\lambda}}_i^H \mathbf{r}_n}{\hat{\boldsymbol{\lambda}}_i^H \hat{\boldsymbol{\lambda}}_i} . \end{aligned} \tag{B.6}$$

The left hand term is considered as a random variable and noted $\hat{f}_{i|-i,s}$ and conditionally to the other parameters it follows a Gaussian distribution of mean $\hat{c}_{i,s}$ and variance $\sigma^2_{i,s} = \frac{\hat{\boldsymbol{\lambda}}_i^{(r)H} \mathbf{S}_f \hat{\boldsymbol{\lambda}}_i^{(r)}}{\left\| \hat{\boldsymbol{\lambda}}_i^{(r)} \right\|_2^4}$, with $\mathbf{S}_f$ as defined in the algorithm. Since the inference targets only $\hat{c}_{i,s}$, the component terms $\hat{c}_{k,s}$ for $k \neq i$ as well as the matrix $\hat{\boldsymbol{\Lambda}}$ are fixed to their previous sample $\hat{\mathrm{c}}_{k,s}^{(r-1)}$ and $\hat{\boldsymbol{\Lambda}}^{(r)}$. A sample of $\hat{f}_{i|-i,s}$ is thus available and noted $\hat{\mathrm{f}}_{i|-i,s}$.
As a consequence, the posterior distribution of $\hat{c}_{i,s}$, $\forall s = 1, \dots, N_{bins}$ and $\forall i = 1, \dots, N_c$ is:

$$\begin{aligned} \text{Likelihood}: \quad & [\hat{\mathrm{f}}_{i|-i,s} | \hat{c}_{i,s}, \sigma^2_{i,s}] \sim \mathcal{N}(\hat{c}_{i,s}, \sigma^2_{i,s}) . \\ \text{Prior}: \quad & [\hat{c}_{i,s} | \hat{\mathrm{c}}^J_{i,s}, \nu^2_{i,s}] \sim \mathcal{N}(\hat{\mathrm{c}}^J_{i,s}, \nu^2_{i,s}) . \end{aligned} \tag{B.7}$$

$$\begin{aligned} [\hat{c}_{i,s}|\text{rest}] &\propto [\hat{\mathrm{f}}_{i|-i,s} | \hat{c}_{i,s}, \sigma^{2\,(r)}_{i,s}] \cdot [\hat{c}_{i,s} | \hat{\mathrm{c}}^J_{i,s}, \nu^{2\,(r-1)}_{i,s}] \\ &\propto \mathcal{N}(\hat{c}_{i,s}, \sigma^2_{i,s}) \cdot \mathcal{N}(\hat{\mathrm{c}}^J_{i,s}, \nu_{i,s}) \\ &\propto \frac{1}{\pi \sigma^{2\,(r)}_{i,s}} \exp\left(-\frac{1}{\sigma^{2\,(r)}_{i,s}} (\hat{\mathrm{f}}_{i|-i,s} - \hat{c}_{i,s})^* (\hat{\mathrm{f}}_{i|-i,s} - \hat{c}_{i,s}) \right) \cdot \\ &\quad \frac{1}{\pi \nu^{2\,(r-1)}_{i,s}} \exp\left(-\frac{1}{\nu^{2\,(r-1)}_{i,s}} (\hat{c}_{i,s} - \hat{\mathrm{c}}^J_{i,s})^* (\hat{c}_{i,s} - \hat{\mathrm{c}}^J_{i,s}) \right) \\ &\propto \exp\left(-\left(\frac{1}{\sigma^{2\,(r)}_{i,s}} + \frac{1}{\nu^{2\,(r-1)}_{i,s}} \right) \hat{c}^*_{i,s} \hat{c}_{i,s} + \hat{c}^*_{i,s} \left(\frac{\hat{\mathrm{f}}_{i|-i,s}}{\sigma^{2\,(r)}_{i,s}} + \frac{\hat{\mathrm{c}}^J_{i,s}}{\nu^{2\,(r-1)}_{i,s}} \right) \right) \cdot \\ &\quad \exp\left(\left(\frac{\hat{\mathrm{f}}^*_{i|-i,s}}{\sigma^{2\,(r)}_{i,s}} + \frac{\hat{\mathrm{c}}^{J\,*}_{i,s}}{\nu^{2\,(r-1)}_{i,s}} \right) \hat{c}_{i,s} \right) . \end{aligned} \tag{B.8}$$

A Gaussian distribution for a random variable x with mean m and covariance s^2 would lead to:

$$[x|\mathrm{m}, \mathrm{s}^2] \propto \exp\left(-\frac{1}{\mathrm{s}^2} x^* x + \frac{1}{\mathrm{s}^2} x^* \mathrm{m} + \frac{1}{\mathrm{s}^2} \mathrm{m}^* x \right) . \tag{B.9}$$

Eqs. (B.8) and (B.9) have the same form and by identification it can be recognised that the posterior distribution of $\hat{c}_{i,s}$ is a Gaussian distribution with parameters:

$$\begin{aligned}\mu_{c_{i,s}} &= \sigma^2_{c_{i,s}} \left(\frac{\hat{f}_{i|-i,s}}{\sigma^{2\,(r)}_{i,s}} + \frac{\hat{c}^J_{i,s}}{\nu^{2\,(r-1)}_{i,s}} \right) \\ \sigma^2_{c_{i,s}} &= \left(\frac{1}{\sigma^{2\,(r)}_{i,s}} + \frac{1}{\nu^{2\,(r-1)}_{i,s}} \right)^{-1} .\end{aligned} \tag{B.10}$$

- Posterior distribution of $\nu^2_{i,s}$, $\forall i = 1, \ldots, N_c$ and $\forall s = 1, \ldots, Nbins$:

$$\begin{aligned}\text{Likelihood}: \quad & [\hat{c}^{(r)}_{i,s} | \hat{c}^J_{i,s}, \nu^2_{i,s}] \sim \mathcal{N}(\hat{c}^J_{i,s}, \nu^2_{i,s}) . \\ \text{Prior}: \quad & [\nu^2_{i,s}] \sim \text{InvGamma}(\alpha_i, \beta_i) .\end{aligned} \tag{B.11}$$

$$\begin{aligned}[\nu^2_{i,s}|\text{rest}] &\propto [\hat{c}^{(r)}_{i,s} | \hat{c}^J_{i,s}, \nu^2_{i,s}][\nu^2_{i,s}] \\ &\propto \mathcal{N}(\hat{c}^J_{i,s}, \nu^2_{i,s}) \cdot \text{InvGamma}(\alpha_i, \beta_i) \\ &\propto \frac{1}{(2\pi\nu^2_{i,s})^{1/2}} \exp\left(-\frac{1}{\nu^2_{i,s}} (\hat{c}^{(r)}_{i,s} - \hat{c}^J_{i,s})^H (\hat{c}^{(r)}_{i,s} - \hat{c}^J_{i,s}) \right) \cdots \\ &\times \frac{\beta_i^{(r-1)\,\alpha_i^{(r-1)}}}{\Gamma(\alpha_i^{(r-1)})} (\nu^2_{i,s})^{-\alpha_i^{(r-1)}-1} e^{-\frac{\beta_i^{(r-1)}}{\nu^2_{i,s}}} \\ &\propto (\nu^2_{i,s})^{-\alpha_i^{(r-1)}-2} \exp\left(-\frac{1}{\nu^2_{i,s}} \left((\hat{c}^{(r)}_{i,s} - \hat{c}^J_{i,s})^H (\hat{c}^{(r)}_{i,s} - \hat{c}^J_{i,s}) + \beta_i^{(r-1)} \right) \right) .\end{aligned}$$

This corresponds to an Inverse-Gamma distribution with parameters $\alpha'_i = \alpha_i^{(r-1)} + 1$ and $\beta'_i = (\hat{c}^{(r)}_{i,s} - \hat{c}^J_{i,s})^H (\hat{c}^{(r)}_{i,s} - \hat{c}^J_{i,s}) + \beta_i^{(r-1)}$.

- Posterior distribution of α_i, $\forall i = 1, \ldots, N_c$:

$$\begin{aligned}\text{Likelihood}: \quad [\boldsymbol{\nu}^{2\,(r)}_{i,:} | \alpha_i, \beta_i] &\sim \prod_{s=1}^{N_{bins}} [\nu^{2\,(r)}_{i,s} | \alpha_i, \beta_i] \\ &\sim \prod_{s=1}^{N_{bins}} \text{InvGamma}(\alpha_i, \beta_i) . \\ \text{Prior}: \quad [\alpha_i] &\sim \text{Exp}(a_\alpha) .\end{aligned} \tag{B.12}$$

$$
\begin{aligned}
[\alpha_i|\text{rest}] &\propto [\boldsymbol{\nu}^{2\,(r)}_{i,:}|\alpha_i, \beta_i^{(r-1)}][\alpha_i] \\
&\propto \prod_{s=1}^{N_{bins}} \text{InvGamma}_{\beta_i^{(r-1)}}(\alpha_i, \beta_i) \cdot \text{Exp}(\mathrm{a}_\alpha) \\
&\propto \prod_{s=1}^{N_{bins}} \frac{\beta_i^{(r-1)\,\alpha_i}}{\Gamma(\alpha_i)} (\nu^{2\,(r)}_{i,s})^{-\alpha_i - 1} \text{exp}\left(-\frac{\beta_i^{(r-1)}}{\nu^{2\,(r)}_{i,s}}\right) \mathrm{a}_\alpha \text{exp}\left(-\mathrm{a}_\alpha \alpha_i\right) \\
&\propto \text{exp}\left(-N_{bins} \ln\left(\Gamma(\alpha_i)\right) + \left(\sum_{s=1}^{N_{bins}} \ln\left(\frac{\beta_i^{(r-1)}}{\nu^{2\,(r)}_{i,s}}\right) - \mathrm{a}_\alpha\right) \alpha_i\right) .
\end{aligned}
\tag{B.13}
$$

This form cannot be recognised as a usual distribution. However, it can be sampled using sampling algorithms such as Metropolis-Hasting [41] or slice sampling [42].

- Posterior distribution of β_i, $\forall i = 1, \ldots, N_c$:

$$
\begin{aligned}
\text{Likelihood}: \quad [\boldsymbol{\nu}^{2\,(r)}_{i,:}|\alpha_i, \beta_i] &\sim \prod_{s=1}^{N_{bins}} [\nu^{2\,(r)}_{i,s}|\alpha_i, \beta_i] \\
&\sim \prod_{s=1}^{N_{bins}} \text{InvGamma}(\alpha_i, \beta_i) . \\
\text{Prior}: \quad [\beta_i] &\sim \text{Gamma}(\mathrm{a}_\beta, \mathrm{b}_\beta) .
\end{aligned}
\tag{B.14}
$$

$$
\begin{aligned}
[\beta_i|\text{rest}] &\propto [\boldsymbol{\nu}^{2\,(r)}_{i,:}|\alpha_i^{(r)}, \beta_i][\beta_i] \\
&\propto \prod_{s=1}^{N_{bins}} \text{InvGamma}_{\alpha_i^{(r)}}(\alpha_i, \beta_i) \cdot \text{Gamma}(\mathrm{a}_\beta, \mathrm{b}_\beta) \\
&\propto \prod_{s=1}^{N_{bins}} \frac{\beta_i^{\alpha_i^{(r)}}}{\Gamma(\alpha_i^{(r)})} (\nu^{2\,(r)}_{i,s})^{-\alpha_i^{(r)} - 1} \text{exp}\left(-\frac{\beta_i}{\nu^{2\,(r)}_{i,s}}\right) \frac{\mathrm{b}_\beta^{\mathrm{a}_\beta}}{\Gamma(\mathrm{a}_\beta)} \beta_i^{\mathrm{a}_\beta - 1} \text{exp}\left(-\mathrm{b}_\beta \beta_i\right) \\
&\propto \beta_i^{\mathrm{a}_\beta - 1 + N_{bins}\alpha_i^{(r)}} \text{exp}\left(-\beta_i \left(\mathrm{b}_\beta + \sum_{s=1}^{N_{bins}} \frac{1}{\nu^{2\,(r)}_{i,s}}\right)\right) .
\end{aligned}
\tag{B.15}
$$

This corresponds to a Gamma distribution with parameters $\mathrm{a}'_\beta = \mathrm{a}_\beta + N_{bins} \cdot \alpha_i^{(r)}$ and $\mathrm{b}'_\beta = \mathrm{b}_\beta + \sum_{s=1}^{N_{bins}} \frac{1}{\nu^{2\,(r)}_{i,s}}$.

Appendix C. Bayesian ICA Algorithm

In what follows the notation $\bullet^H$ stands for the Hermitian transpose, $\bullet^t$ for the matrix transpose, $\bullet^*$ for the complex conjugate and "rest" stands for all the random variables

but for the one whose posterior PDF is being expressed. The samples of the random variables are noted with upright letters, such as $\mathbf{c}^{(r)}$ or $\alpha_i^{(r)}$, with r standing for the r^{th} sample in the iterative algorithm. For the analytic form of usual PDFs refer to Appendix A, whereas for the computations leading to this algorithm refer to Appendix B.

The proposed Bayesian ICA consists of 10 steps:

1. Initialize the values of $\hat{\mathbf{\Lambda}}^{(0)}$, $\hat{\mathbf{C}}^{(0)}$, $\forall i = 1, \ldots, N_c$ and $\forall s = 1, \ldots, N_{bins}$, $\nu_{i,s}^{2\,(0)}$ and $\forall i = 1, \ldots, N_c$, $\beta_i^{(0)}$ and $\alpha_i^{(0)}$.
   For all $r = 1, \ldots, N_{run}$, do:

2. Generate an input $\hat{\mathbf{F}}^{(r)}$ out of the structure $\{\tilde{\mathbf{F}}\}$. It can be generated as:

$$\forall s = 1, \ldots, N_{bins}, \quad \hat{\mathbf{F}}_{:,s}^{(r)} = \tilde{\mathbf{F}}_{:,z_s^{(r)}}^{(s)}, \tag{C.1}$$

   where $z_s^{(r)}$ is a sample from a discrete uniform distribution defined on $\{1, \ldots, N_s^{(s)}\}$.

3. $\forall j = 1, \ldots, N_e$, $\forall s = 1, \ldots, N_{bins}$, draw a sample $\sigma_{f_{j,s}}^{2\,(r)}$ from $[\sigma_{f_{j,s}}^2 | \text{rest}] \sim \text{InvGamma}(\alpha'_f, \beta'_f)$ with

$$\begin{aligned} \alpha'_f &= \alpha_f + 1 \\ \beta'_f &= \beta_f + |\hat{f}_{j,s}^{(r)} - \hat{\mathbf{l}}_j^{(r-1)} \hat{\mathbf{c}}_s^{(r-1)}|^2, \end{aligned} \tag{C.2}$$

   where $\hat{f}_{j,s}^{(r)}$ is a term out of the matrix $\hat{\mathbf{F}}^{(r)}$, while $\hat{\mathbf{l}}_j^{(r-1)}$ is the j^{th} row of the *pattern* matrix $\hat{\mathbf{\Lambda}}^{(r-1)}$ and $\hat{\mathbf{c}}_s^{(r-1)}$ the s^{th} column of the component matrix $\hat{\mathbf{C}}^{(r-1)}$.

4. $\forall j \in [1, \ldots, N_e]$, draw a sample $\hat{\mathbf{l}}_j^{t\,(r)}$ from $[\hat{\ell}_j^t | \text{rest}] \sim \mathcal{N}(\boldsymbol{\mu}_{l_j}, \boldsymbol{\Sigma}_{l_j})$ with

$$\begin{aligned} \boldsymbol{\mu}_{l_j} &= \boldsymbol{\Sigma}_{l_j} \hat{\mathbf{C}}^{(r-1)\,*} \boldsymbol{\Sigma}_f^{-1} \hat{\mathbf{f}}_j^{(r)\,t} \\ \boldsymbol{\Sigma}_{l_j} &= ((\hat{\mathbf{C}}^{(r-1)} \boldsymbol{\Sigma}_f^{-1} \hat{\mathbf{C}}^{(r-1)\,H})^*)^{-1}, \end{aligned} \tag{C.3}$$

   with $\boldsymbol{\Sigma}_f = \text{diag}(\sigma_{f_{j,1}}^{2\,(r)}, \ldots, \sigma_{f_{j,N_{bins}}}^{2\,(r)})$.

5. Normalize the columns of $\hat{\mathbf{\Lambda}}^{(r)}$ to 1 to solve the indeterminacy on gain.

6. $\forall i = 1, \ldots, N_c$ and $\forall s = 1, \ldots, N_{bins}$, draw a sample $\hat{c}_{i,s}^{(r)}$ from $[\hat{c}_{i,s} | \text{rest}] \sim \mathcal{N}(\mu_{c_{i,s}}, \sigma_{c_{i,s}}^2)$

with

$$\begin{aligned}
\mu_{c_{i,s}} &= \sigma^2_{c_{i,s}} \left(\frac{\hat{f}^{(r)}_{i|-i,s}}{\sigma^2_{i,s}} + \frac{\hat{c}^{J}_{i,s}}{\nu^{2\,(r-1)}_{i,s}} \right) \\
\sigma^2_{c_{i,s}} &= \left(\frac{1}{\sigma^2_{i,s}} + \frac{1}{\nu^{2\,(r-1)}_{i,s}} \right)^{-1} \\
\sigma^2_{i,s} &= \frac{\hat{\boldsymbol{\lambda}}^{(r)\,H}_{i} \mathbf{S}_f \hat{\boldsymbol{\lambda}}^{(r)}_{i}}{\left\| \hat{\boldsymbol{\lambda}}^{(r)}_{i} \right\|^4_2} \\
\hat{f}^{(r)}_{i|-i,s} &= \frac{\hat{\boldsymbol{\lambda}}^{(r)\,H}_{i} \hat{\mathbf{f}}^{(r)}_{s}}{\hat{\boldsymbol{\lambda}}^{(r)\,H}_{i} \hat{\boldsymbol{\lambda}}^{(r)}_{i}} - \sum_{k \neq i} \frac{\hat{\boldsymbol{\lambda}}^{(r)\,H}_{i} \hat{\boldsymbol{\lambda}}^{(r)}_{k}}{\hat{\boldsymbol{\lambda}}^{(r)\,H}_{i} \hat{\boldsymbol{\lambda}}^{(r)}_{i}} \hat{c}^{(r-1)}_{k,s},
\end{aligned} \tag{C.4}$$

with $\mathbf{S}_f = \mathrm{diag}(\sigma^{2\,(r)}_{f_{1,s}}, \ldots, \sigma^{2\,(r)}_{f_{N_e,s}})$ and $\hat{\boldsymbol{\lambda}}^{(r)}_{i}$ standing for the i^{th} column of the *pattern* matrix $\hat{\boldsymbol{\Lambda}}^{(r)}$.

7. $\forall i = 1, \ldots, N_c$ and $\forall s = 1, \ldots, N_{bins}$, draw a sample $\nu^{2\,(r)}_{i,s}$ from $[\nu^2_{i,s}|\mathrm{rest}] \sim \mathrm{InvGamma}(\alpha'_{i,s}, \beta'_{i,s})$ with

$$\begin{aligned}
\alpha'_{i,s} &= \alpha^{(r-1)}_{i} + 1 \\
\beta'_{i,s} &= \beta^{(r-1)}_{i} + |\hat{c}^{(r)}_{i,s} - \hat{c}^{J}_{i,s}|^2 .
\end{aligned} \tag{C.5}$$

8. $\forall i = 1, \ldots, N_c$, draw a sample $\alpha^{(r)}_{i}$ from

$$[\alpha_i|\mathrm{rest}] \propto \exp\left(-N_{bins} \log\Gamma(\alpha_i) + \left(\sum_{s=1}^{N_{bins}} \log \frac{\beta^{(r-1)}_{i}}{\nu^{2\,(r)}_{i,s}} - a_\alpha \right) \alpha_i \right) . \tag{C.6}$$

This distribution is obtained by Bayes theorem as the product of an Inverse Gamma distribution by an exponential distribution (see Appendix B) and it is not easy to sample. A Metropolis-Hastings sampler might be needed. In practice, since α_i is high in the hierarchy (see Fig. 8) deterministic moves are found to not compromise the convergence of the Markov Chain. As a consequence, the mode of the distribution is chosen as sample at each iteration:

$$\begin{aligned}
\alpha^{(r)}_{i} &= \underset{\alpha_i}{\mathrm{argmax}} \left(-N_{bins} \log\Gamma(\alpha_i) + \left(\sum_{s=1}^{N_{bins}} \log \frac{\beta^{(r-1)}_{i}}{\nu^{2\,(r)}_{i,s}} - a_\alpha \right) \alpha_i \right) \\
&= \psi^{-1} \left(\frac{1}{N_{bins}} \left(\sum_{s=1}^{N_{bins}} \log \frac{\beta^{(r-1)}_{i}}{\nu^{2\,(r)}_{i,s}} - a_\alpha \right) \right) ,
\end{aligned} \tag{C.7}$$

where $\psi^{-1}(\bullet)$ is the *inverse Digamma function*.

9. $\forall i = 1, \ldots, N_c$, draw a sample $\beta_i^{(r)}$ from $[\beta_i|\text{rest}] \sim \text{Gamma}(a'_\beta, b'_\beta)$ with

$$\begin{aligned} a'_\beta &= a_\beta + N \cdot \alpha_i^{(r)} \\ b'_\beta &= b_\beta + \sum_{s=1}^{N_{bins}} \frac{1}{\nu_{i,s}^{2\,(r)}} . \end{aligned} \tag{C.8}$$

10. Check the convergence and set the number of iterations N_{run} in order to collect a sufficiently large sample of the random variables after the convergence of the Markov chain.

The proposed algorithm is built upon the one developed by Fevotte [43], but it presents some major differences. First of all, it works on complex quantities unlike the former version which is valid only for real signals. This entails some modified expression and an indeterminacy on the phase of the result. While the indeterminacy on the amplitude is solved by normalizing the columns of the pattern matrix (step 5), the determination of the phase is performed naturally thanks to the prior distributions. Moreover, step 2 is specific to the proposed algorithm. The aim here is to make the algorithm explore all possible input samples, in order to propagate the uncertainty described by the structure $\{\tilde{\mathbf{F}}\}$ to the results of the ICA.

Appendix D. OC Modelling algorithm

The algorithm is detailed for $\hat{\mathbf{C}}^{mod}$, but is exactly equivalent when applied to the phase. It is the following:

1. Let $\mathbf{O} \in \mathbb{R}^{N_{OC} \times N_{bins}}$ be the matrix of the predictor variables. Here, it contains the engine torque and speed corresponding to the active bins of the manifold $\mathcal{O}'$. As a consequence, $N_{OC} = 2$.

2. Apply the MATLAB function *newrb(...)*, with arguments $\mathbf{O}$, $\mathbf{C}^{mod}$, g and v. The mean squared error g allows to control the dimension of the model, while the spread v its regularity. This function yields the number of RBF N_{rb} and for each $b \in \{1, \ldots, N_{rb}\}$ their position $\boldsymbol{\mu}_b \in \mathbb{R}^{N_{OC} \times 1}$ and variance $\sigma_b^2 \in \mathbb{R}$.

3. Compute the radial basis $\mathbf{X} \in \mathbb{R}^{N_{rb} \times N_{bins}}$ where each component of the matrix reads:

$$\begin{aligned} &\forall b = 1, \ldots, N_{rb}, \quad \forall s = 1, \ldots, N_{bins} \\ &X_{b,s} = e^{-\frac{1}{\sigma_b^2} ||\boldsymbol{\mu}_b - \mathbf{o}_s||^2} , \end{aligned} \tag{D.1}$$

   where $\mathbf{o}_s$ is the s^{th} column of matrix $\mathbf{O}$. Note that in the MATLAB function and thereof in this application, the radial function $\phi(r)$ is a Gaussian function.

4. Initialize the values of $\mathbf{W}^{(0)}$, $\forall i = 1, \ldots, N_c$ and $\forall s = 1, \ldots, N_{bins}$, $\sigma_{c_{i,s}}^{2\,(0)}$ and $\forall i = 1, \ldots, N_c$ and $\forall b = 1, \ldots, N_{rb}$, $\sigma_{w_{i,b}}^{2\,(0)}$.
   For all $r = 1, \ldots, N_{run}$, do:

5. Draw a component sample from the structure $\{\hat{\mathbf{C}}\}$, as $\hat{\mathbf{C}}^{(z^{(r)})}$, where $z^{(r)}$ is a sample from a discrete uniform distribution defined on $\{1, \ldots, N_{run}\}$. Using this sample, compute $\hat{\mathbf{C}}^{mod\,(r)}$ as in Eq. (23).

6. $\forall i = 1, \ldots, N_c, \forall s = 1, \ldots, N_{bins}$, draw a sample $\sigma^{2\,(r)}_{c_{i,s}}$ from $[\sigma^2_{c_{i,s}}|\text{rest}] \sim \text{InvGamma}(\alpha'_c, \beta'_c)$ with

$$\begin{aligned} \alpha'_c &= \alpha_c + 1/2 \\ \beta'_f &= \beta_f + 1/2|\hat{c}^{mod\,(r)}_{i,s} - \mathbf{w}^{(r-1)}_i \mathbf{x}_s|^2 \,, \end{aligned} \tag{D.2}$$

where $\hat{c}^{mod\,(r)}_{i,s}$ is a term out of the matrix $\hat{\mathbf{C}}^{mod\,(r)}$, while $\mathbf{w}^{(r-1)}_i$ is the i^{th} row of the weight matrix $\mathbf{W}^{(r-1)}$ and $\mathbf{x}_s$ the s^{th} column of the predictor matrix $\mathbf{X}$.

7. $\forall i = 1, \ldots, N_c$, draw a sample $\mathbf{w}^{t\,(r)}_i$ from $[\boldsymbol{w}^t_i|\text{rest}] \sim \mathcal{N}(\boldsymbol{\mu}_{w_i}, \boldsymbol{\Sigma}_{w_i})$ with

$$\begin{aligned} \boldsymbol{\mu}_{w_i} &= \boldsymbol{\Sigma}_{w_i} \mathbf{X} \boldsymbol{\Sigma}_c^{-1} (\hat{\mathbf{c}}^{mod\,(r)}_i)^t \\ \boldsymbol{\Sigma}_{w_i} &= (\mathbf{X} \boldsymbol{\Sigma}_c^{-1} \mathbf{X}^t + \mathbf{S}_w^{-1})^{-1} \,, \end{aligned} \tag{D.3}$$

with $\boldsymbol{\Sigma}_c = \text{diag}(\sigma^{2\,(r)}_{c_{i,1}}, \ldots, \sigma^{2\,(r)}_{c_{i,N_{bins}}})$ and $\mathbf{S}_w = \text{diag}(\sigma^{2\,(r-1)}_{w_{i,1}}, \ldots, \sigma^{2\,(r-1)}_{w_{i,N_{rb}}})$.

8. $\forall i = 1, \ldots, N_c$ and $\forall b = 1, \ldots, N_{rb}$, draw a sample $\sigma^{2\,(r)}_{w_{i,b}}$ from $[\sigma^2_{w_{i,b}}|\text{rest}] \sim \text{InvGamma}(\alpha'_{i,b}, \beta'_{i,b})$ with

$$\begin{aligned} \alpha'_{i,b} &= \alpha_w + 1/2 \\ \beta'_{i,b} &= \beta_w + 1/2|\mathrm{w}^{(r)}_{i,b}|^2 \,. \end{aligned} \tag{D.4}$$

9. Check the convergence and set the number of iterations N_{run} in order to collect a sufficiently large sample of the random variables after the convergence of the Markov chain.

References

[1] E. Winklhofer, G. E. Thien, A review of parameters affecting the noise and vibration in diesel powered passenger cars, Tech. rep., SAE Technical Paper (1985).

[2] S.-K. Lee, H. C. Chae, The application of artificial neural networks to the characterization of interior noise booming in passenger cars, Proceedings of the Institution of Mechanical Engineers, Part D: Journal of Automobile Engineering 218 (1) (2004) 33–42.

[3] S.-H. Shin, J.-G. Ih, T. Hashimoto, S. Hatano, Sound quality evaluation of the booming sensation for passenger cars, Applied acoustics 70 (2) (2009) 309–320.

[4] N. Lalor, H.-H. Priebsch, The prediction of low-and mid-frequency internal road vehicle noise: a literature survey, Proceedings of the Institution of Mechanical Engineers, Part D: Journal of Automobile Engineering 221 (3) (2007) 245–269.

[5] Q. Leclere, L. Polac, B. Laulagnet, J.-L. Guyader, Vibro-acoustique des moteurs d'automobile (vibroacoustics of automotive engines), Techniques de l'Ingenieur (2006) BM–2.

[6] Y. Yu, N. G. Naganathan, R. V. Dukkipati, A literature review of automotive vehicle engine mounting systems, Mechanism and machine theory 36 (1) (2001) 123–142.

[7] A. Carrella, Nonlinear identifications using transmissibility: Dynamic characterisation of anti vibration mounts (avms) with standard approach and nonlinear analysis, International Journal of Mechanical Sciences 63 (1) (2012) 74–85.

[8] G. Brogna, J. Antoni, N. Totaro, L. Gagliardini, O. Sauvage, Modelling vehicles nvh performances: a probabilistic approach., in: INTER-NOISE and NOISE-CON Congress and Conference Proceedings, Vol. 255, Institute of Noise Control Engineering, Hong Kong, China, 27 – 30 August 2017, pp. 1400–1411.

[9] J.-F. Durand, C. Soize, L. Gagliardini, Structural-acoustic modeling of automotive vehicles in presence of uncertainties and experimental identification and validation, The Journal of the Acoustical Society of America 124 (3) (2008) 1513–1525.

[10] J. Antoni, Blind separation of vibration components: Principles and demonstrations, Mechanical Systems and Signal Processing 19 (6) (2005) 1166–1180.

[11] J. Antoni, S. Chauhan, A study and extension of second-order blind source separation to operational modal analysis, Journal of Sound and Vibration 332 (4) (2013) 1079–1106.

[12] I. G. Araújo, J. A. García Sánchez, P. Andersen, Modal parameter identification based on combining transmissibility functions and blind source separation techniques, Mechanical Systems and Signal Processing 105 (2018) 276–293.

[13] N. Saito, B. Bénichou, The spike process: a simple test case for independent or sparse component analysis, in: Proc. 3rd International Conference on Independent Component Analysis and Signal Separation, T.-W. Lee, T.-P. Jung, S. Makeig, and TJ Sejnowski, eds., IEEE, San Diego, California, 9-13 December 2001, pp. 698–703.

[14] N. Saito, The generalized spike process, sparsity, and statistical independence, Modern signal processing 46 (2004) 317–340.

[15] K. H. Knuth, A bayesian approach to source separation, arXiv preprint physics/0205032.

[16] A. Mohammad-Djafari, A bayesian approach to source separation, in: AIP Conference proceedings, Bayesian Inference and Maximum Entropy Methods in Science and Engineering: 19th International Workshop, Vol. 567, AIP, Boise, Idaho, 2-5 Aug 1999, pp. 221–244.

[17] D. S. Broomhead, D. Lowe, Radial basis functions, multi-variable functional interpolation and adaptive networks, Tech. rep., DTIC Document (1988).

[18] M. J. Gander, L. Halpern, Méthodes de décomposition de domaines - notions de base (methods for domain decomposition – basic notions), Techniques de l'ingénieur.

[19] M. V. Van der Seijs, D. de Klerk, D. J. Rixen, General framework for transfer path analysis: History, theory and classification of techniques, Mechanical Systems and Signal Processing 68 (2016) 217–244.

[20] A. Gaudin, J. F. Beniguel, Low frequency road noise decomposition at wheel center on an roller bench, in: Proceedings of the Acoustics 2012 Conference, Nantes, France, 23-27 April 2012.

[21] D. D. van den Bosch, M. V. van der Seijs, D. de Klerk, Validation of blocked-force transfer path analysis with compensation for test bench dynamics, in: Dynamics of Coupled Structures, Volume 1, Proceedings of the 32nd IMAC, A Conference and Exposition on Structural Dynamics, Springer International Publishing, Houghton, MI, 2014, pp. 37–49.

[22] A. T. Moorhouse, A. S. Elliott, T. A. Evans, In situ measurement of the blocked force of structure-borne sound sources, Journal of Sound and Vibration 325 (4-5) (2009) 679–685.

[23] A. S. Elliott, A. T. Moorhouse, T. Huntley, S. Tate, In-situ source path contribution analysis of structure borne road noise, Journal of Sound and Vibration 332 (24) (2013) 6276–6295.

[24] A. Thite, D. Thompson, The quantification of structure-borne transmission paths by inverse methods. part 1: Improved singular value rejection methods, Journal of Sound and Vibration 264 (2) (2003) 411–431.

[25] A. Thite, D. Thompson, The quantification of structure-borne transmission paths by inverse methods. part 2: Use of regularization techniques, Journal of Sound and Vibration 264 (2) (2003) 433–451.

[26] D. Calvetti, E. Somersalo, An Introduction to Bayesian Scientific Computing: Ten Lectures on Subjective Computing, Vol. 2, Springer Science & Business Media, New York, NY, 2007.

[27] M. Aucejo, O. De Smet, On a full bayesian inference for force reconstruction problems, Mechanical Systems and Signal Processing 104 (2018) 36–59. doi:https://doi.org/10.1016/j.ymssp.2017.10.023.
URL https://www.sciencedirect.com/science/article/pii/S0888327017305538

[28] W. Feng, Q. Li, Q. Lu, B. Wang, C. Li, Time domain force localization and reconstruction based on hierarchical bayesian method, Journal of Sound and Vibration 472 (2020) 115222. doi:https://doi.org/10.1016/j.jsv.2020.115222.
URL https://www.sciencedirect.com/science/article/pii/S0022460X20300535

[29] G. Brogna, J. Antoni, N. Totaro, L. Gagliardini, O. Sauvage, Identification of sources through a probabilistic approach: application to vehicles in real usage conditions., in: NOVEM Conference Proceedings, Ibiza, Spain, 7 – 9 May 2018.

[30] T. ten Wolde, J. W. Verheij, H. F. Steenhoek, Reciprocity method for the measurement of mechano-acoustical transfer functions, Journal of Sound and Vibration 42 (1) (1975) 49–55.
[31] A. Hyvärinen, J. Karhunen, E. Oja, Independent component analysis, Vol. 46, John Wiley & Sons, New York, NY, 2004.
[32] H. Hotelling, Analysis of a complex of statistical variables into principal components, Journal of educational psychology 24 (6) (1933) 417–441.
[33] T. Eltoft, T. Kim, T.-W. Lee, Multivariate scale mixture of gaussians modeling, in: International Conference on Independent Component Analysis and Signal Separation, Springer, Charleston, SC, 5-8 March 2006, pp. 799–806.
[34] W. M. Bolstad, Understanding computational Bayesian statistics, Vol. 644, John Wiley & Sons, New York, NY, 2010.
[35] J.-F. Cardoso, A. Souloumiac, Blind beamforming for non-gaussian signals, in: IEE proceedings F (radar and signal processing), Vol. 140, IET, 1993, pp. 362–370.
[36] S. Geman, D. Geman, Gibbs distributions, and the bayesian restoration of images, IEEE Transactions on Pattern Analysis and Machine Intelligence 6 (1984) 721–741.
[37] A. Gelman, D. B. Rubin, Inference from iterative simulation using multiple sequences, Statistical science (1992) 457–472.
[38] E. Viennet, Réseaux à fonctions de base radiales (radial basis networks), in: Apprentissage Connexionniste, Lavoisier, Paris, France, 2006, Ch. 4.
[39] J. Moody, C. J. Darken, Fast learning in networks of locally-tuned processing units, Neural computation 1 (2) (1989) 281–294.
[40] R. M. Neal, Slice sampling, Annals of statistics (2003) 705–741.
[41] W. K. Hastings, Monte carlo sampling methods using markov chains and their applications, Biometrika 57 (1) (1970) 97–109.
[42] C. M. Bishop, Pattern recognition and machine learning, springer, New York, NY, 2006.
[43] C. Févotte, Bayesian audio source separation, Blind Speech Separation (2007) 305–335.

Declaration of interests

☒ The authors declare that they have no known competing financial interests or personal relationships that could have appeared to influence the work reported in this paper.

☐The authors declare the following financial interests/personal relationships which may be considered as potential competing interests:

Jérôme Antoni, on behalf of all (co)authors
27 July 2020

Gianluigi Brogna: Methodology ; Software ; Validation; Formal analysis ; Investigation; Writing - Original Draft; Writing - Review & Editing ; Visualization

Jérôme Antoni: Resources ; Writing - Review & Editing; Supervision; Project administration

Nicolas Totaro: Resources ; Writing - Review & Editing; Supervision

Olivier Sauvage: Resources ; Data Curation ; Supervision ; Project administration ; Funding acquisition

Laurent Gagliardini: Resources ; Data Curation ; Supervision